EXPERIMENTAL INVESTIGATION OF DRAG REDUCTION EFFECTS OF POLYMER ADDITIVES ON TURBULENT PIPE FLOW

A THESIS SUBMITTED TO
THE GRADUATE SCHOOL OF NATURAL AND APPLIED SCIENCES
OF
MIDDLE EAST TECHNICAL UNIVERSITY

BY

ŞERİFE ZEYBEK

IN PARTIAL FULFILLMENT OF THE REQUIREMENTS

FOR

THE DEGREE OF MASTER OF SCIENCE

IN

CHEMICAL ENGINEERING

AUGUST 2005

Approval of the Graduate School of Natural and Applied Science

Prof. Dr. Canan ÖZGEN
Director

I certify that this thesis satisfies all the requirements as a thesis for the degree of Master of Science

Prof. Dr. Nurcan BAÇ
Head of Department

This is to certify that we have read this thesis and that in our opinion it is fully adequate, in scope and quality, as a thesis for the degree of Master of Science

Assoc. Prof. Dr. Göknur BAYRAM
Co-Supervisor

Assist. Prof. Dr. Yusuf ULUDAĞ
Supervisor

Examining Committee Members

Prof. Dr. Timur DOĞU (METU, CHE)

Assist. Prof. Dr. Yusuf ULUDAĞ (METU, CHE)

Assoc. Prof. Dr. Göknur BAYRAM (METU, CHE)

Assist. Prof. Dr. Halil KALIPÇILAR (METU, CHE)

Assoc. Prof. Dr. Serkan ÖZGEN (METU, AEE)

I hereby declare that all information in this document has been obtained and presented in accordance with academic rules and ethical conduct. I also declare that, as required by these rules and conduct, I have fully cited and referenced all material and results that are not original to this work.

Name, Last name : Şerife Zeybek

Signature :

ABSTRACT

EXPERIMENTAL INVESTIGATION OF DRAG REDUCTION EFFECTS OF

POLYMER ADDITIVES ON TURBULENT PIPE FLOW

Zeybek, Şerife
M.S., Department of Chemical Engineering
Supervisor : Assist. Prof. Dr. Yusuf Uludağ
Co-Supervisor: Assoc. Prof. Dr. Göknur Bayram

August 2005, 82 pages

Since the discovery of the drag reduction effects of even small amount of macromolecules in solutions in turbulent pipe flows, there have been many experimental and theoretical studies in order to understand mechanisms behind this phenomenon. Theories have been proposed based on the observations on the change in the characteristics of the turbulent flow near the pipe wall where friction of the momentum transfer between the flow and the conduit takes place.

In this study drag reduction in fully developed turbulent pipe flow with four concentrations (200 to 500 wppm) of low molecular weight Sodium Carboxymethylcellulose (CMC) in aqueous solutions was investigated experimentally. Drag reduction was determined by pressure drop measurements. In order to observe the impact of the presence of CMC on the flow, Ultrasound Doppler Velocimetry (UDV) was employed to monitor the instantaneous velocity distributions. UDV is a non-invasive technique allowing one to obtain quick velocity profiles. Experimental measurements were used to calculate Fanning friction factor

and radial distributions of the axial time-averaged velocity, velocity fluctuation (turbulent intensity) and eddy viscosity.

The drag reduction level was determined through the Fanning friction factor versus Reynolds number data. Velocity data could be obtained as close as 3 mm to the wall by UDV.

Two impacts of increasing CMC concentration on the flow field, hence pressure drop, were observed. The first effect was the decrease of the mean velocity gradient especially near the wall with increasing polymer amount which in turn gave rise to lower friction factor or pressure drop. In addition smaller eddy viscosities were obtained in the flow. The second impact of the polymer addition was on the velocity fluctuation or turbulent intensity variation along the radial distribution. An increasing trend in turbulence intensity in the turbulent core with polymer addition was observed. This was in agreement with the earlier studies in which similar turbulence behavior was observed in addition to the suppression of the turbulent intensities near the wall

Keywords: Ultrasound Doppler Velocimetry, Turbulent Pipe Flow, Water Soluble Polymers, Drag Reduction

ÖZ

POLİMER KATKI MADDELERİNİN TÜRBÜLENT BORU AKIŞINDA

SÜRTÜNME AZALTICI ETKİLERİNİN DENEYSEL OLARAK İNCELENMESİ

Zeybek, Şerife
Yüksek Lisans, Kimya Mühendisliği Bölümü
Tez Yöneticisi :Yrd. Doç. Dr. Yusuf Uludağ
Ortak Tez Yöneticisi : Doç. Dr. Göknur Bayram

Ağustos 2005, 82 sayfa

Çözelti içindeki az miktarda polimerin türbülent boru akışında sürtünme kaybına neden olduğunun keşfedilmesinden beri, bu olayın arkasında yatan mekanizmayı anlamak için birçok deneysel ve teorik çalışma gerçekleştirilmiştir. Teoriler, akışla sistem arasındaki momentum transferinin ve sürtünmenin yer aldığı boru duvarı yakınında, türbülent akış karakteristiğinde meydana gelen değişimlerin gözlenmesine dayanılarak önerilmişitir. Bu çalışmada, düşük molekül ağırlıklı Sodyum Karboksimetilselüloz polimerinin dört farklı konsantrasyonda (200 wppm'den 500 wppm'e) hazırlanmış sulu çözeltilerinin, tam gelişmiş türbülent akışta sürtünme azaltıcı etkileri deneysel olarak incelendi. Sürtünme azalması, basınç düşmesi ölçümleriyle belirlendi. Polimerlerin akış üzerindeki etkisini gözlemlemek için anlık hız dağılımları Ultrasound Doppler Velocimetry (UDV) ile görüntülendi. UDV kısa zamanda hız profili ölçümleri almayı sağlayan, sistemi rahatsız etmeyen bir tekniktir. Deneysel ölçümler, Fanning sürtünme faktörü ve eksenel zaman ortalamalı hız, hız dalgalanmaları ve eddy viskozite verilerinin radyal yöndeki dağılımlarının hesaplanmasında kullanıldı.

Sürtünme azalmasının derecesi, Fanning sürtünme faktörüne karşı Reynolds sayısı verilerinden tanımlandı. Hız verileri UDV tarafından, duvarın 3 mm yakınından itibaren elde edilebildi.

Artan polimer derişiminin akış alanı, dolayısıyla sürtünme üzerinde iki etkisi gözlemlendi. İlk etki, daha düşük sürtünme faktörüne veya basınç düşmesine neden olan artan polimer miktarı ile, özellikle duvar yakınında ortalama hız gradientinin düşmesiydi. Ek olarak akış içinde daha küçük eddy viskozite değerleri elde edildi. Polimer eklemenin ikinci etkisi, hız dalgalanmalarının veya türbülent şiddetinin radyal dağılım boyunca değişimiydi. Türbülans şiddetinin, türbülent iç bölgede polimer eklenmesiyle arttığı gözlendi. Bu sonuç, benzer türbülans davranışı gösteren ve duvar kenarındaki hız dalgalanmalarının baskı altına alındığı daha önceki çalışmalarla uygunluk gösteriyor.

Anahtar Sözcükler: Ultrasound Doppler Velocimetry, Türbülent Boru Akışı, Suda Çözünebilir Polimerler, Sürtünme Azalması.

To my family

ACKNOWLEDGMENTS

I wish to express my deepest gratitude to my supervisor Assist. Prof. Dr. Yusuf Uludağ and co-supervisor Assoc. Prof. Dr. Göknur Bayram for their guidance, advice, criticism, encouragements and insight throughout the research.

I am indebted to my dear parents for their continuous encouragement, understanding and their endless support during my life.

I am very thankful to my dear friends Barış Vural and Volkan Köseli for their help and support.

TABLE OF CONTENTS

LIST OF TABLES

TABLES

LIST OF FIGURES

FIGURES

NOMENCLATURE

C = concentration of polymer solution weight parts per million (wppm)

D = pipe diameter (m)

DR = drag reduction

f = Fanning's friction factor

g = gravity constant

Δh = length difference at manometer (m)

ΔP = pressure difference (Pa)

Q = volumetric flow rate (l/s)

r = distance from pipe centre (m)

R = radius of pipe (m)

Re = Reynolds number

$\bar{U}$ = time average velocity (mm/s)

U* = friction velocity

u' = axial turbulent velocity fluctuation

u^+ = normalized time average velocity by friction velocity

<V> = average bulk flow velocity (m/s)

Δx = pipe length between pressure taps (m)

y = distance from pipe wall (m)

y^+ = normalized radial distance

Greek Letters

Δ = difference between the data

ε = eddy viscosity (Pa.s)

μ = dynamic viscosity (Pa.s)

ν = kinematic viscosity

ρ = density (kg/m^3)

τ = shear stress (Pa)

Subscripts

m = fluid of manometer

o = center of pipe

p = polymer (CMC) solution

rms = root mean square

s = solvent (water)

t = turbulent

v = viscous

w = at the wall

CHAPTER 1

INTRODUCTION

Addition of small amount of (tens of parts per million by weight) polymers to the flow system results in the reduction of skin friction in turbulent flow. This phenomenon is known as 'Drag Reduction' and was discovered by Toms in 1949, therefore can be termed as 'Toms Phenomenon'. Since that time, the interest on drag reduction has grown because of its wide range of industrial applications. Despite large number of experimental and theoretical studies on this area over half a century, an exact mechanism explaining the phenomenon has not been yet obtained due to the complexity of its physics.

Drag reduction additives can be classified in three categories: high and low molecular weight polymers, cationic-anionic-zwitterionic surfactants and fibers (Myska et al. 2001). Among these, the most effective drag reducer is the high molecular weight polymers, but their high degradation rate decreases the effectiveness in the recirculation systems. Surfactant additives also suffer from temporary mechanical and thermal degradations, but they have the capability of 'repairing' themselves in the order of seconds (Yu et al, 2004).

Virk et al. (1967) studied experimentally drag reduction on turbulent pipe of dilute polymer solutions and reported that the onset of drag reduction occurs at a well defined wall shear stresses related to the random coiling effective diameter of the polymer. Laminar to the turbulent transition is not, in general delayed. The extent of drag reduction induced by a homologous series of polymers in a given pipe is a universal function of concentration, flow rate, and molecular weight. The maximum

drag reduction possible is limited by an asymptote that is independent of polymer and pipe diameter.

Various mechanisms of drag reduction have been proposed in the literature. The most common one is the Lumley Theory. Lumley (1973) emphasized that viscoelastic effect occurs when the hydrodynamic frequencies become higher than the relaxation rate of one coil. For turbulent flow, outside the viscous sublayer polymer chains are stretched by turbulence because of the increasing strain rate in the turbulence and this causes enhanced effective viscosity in the turbulent region. On the other hand, the viscosity in the viscous sublayer remains low. But, Lumley did not give the detailed experimental results and theoretical models supporting the mechanism. Therefore, Hinch (1977), suggested polymer elongation models to show the elongation of polymer molecule results in an increase of the effective viscosity theoretically. A 'two-scale model' was used to analyze the effect of the localized turbulence production. This model proposed that the small-scale motions produced by secondary inflectional instability were the source the large-scale motions through the creation of localized Reynolds stresses resulting from the small-scale mixing. In their study, elastic effect of dilute polymer solutions had not been studied. Thus, De Gennes (1986) investigated the energy exchange between the kinetic and elastic energy in the core of the turbulent flow, far from the boundary. He concluded that the polymer effect at small scales (high frequencies) is not described by a viscosity, but by an 'elastic modulus'. Flexible polymers in dilute solutions enhance the viscosity in slow flows. But in strong, rapidly varying, shear fields, they behave elastically. A turbulent cascade (from large to small scales) should thus be deeply modified when the elastic stresses become comparable to the Reynolds stress.

The roles of stress anisotropy and of elasticity in the mechanism of drag reduction by polymer additives were investigated by Den Toonder et al. (1997). The investigation was carried out by means of direct numerical simulation (DNS) and laser Doppler velocimetry (LDV). In DNS two different models were used and the first model based on the viscous anisotropic effects, the second model was the extension of the first model with an elastic component. For the case of viscous anisotropic polymer

model, calculated data agreed in qualitative sense with the LDV measurements, the viscoelastic polymer model showed less drag reduction than the anisotropic model without elasticity. Thus, they claimed that viscous anisotropic stresses introduced by extent of polymers play a key role in the mechanism of drag reduction (Den Toonder et al. 1997).

The drag reduction experiments have focused on homogeneous (premixed) polymer solutions and it is thought that the interaction between polymer molecules and turbulent structure observed near the wall is responsible for the drag reduction. To check whether or not polymer drag reduction is a phenomenon taking place exclusively in the near wall region, the heterogeneous drag reduction in which the concentrated polymer solutions are injected into a turbulent pipe flow was examined. According to the study performed by Warholic et al. (1999), drag reduction does not only depend on the mixed concentration in the test section. The method of injection and inconsistencies in the preparation of the concentrated solutions also appear to be having strong effects. For example, injected polymer solutions had concentrations that varied from 50 to 2000 wppm and flow rates, from 0.7 to 30 L/min, after the experiments a range of drag reduction of 10-69% was obtained. It was reported that the thickness of the viscous sublayer increases with increasing drag reduction and velocity profiles for drag reduction are consistent with Lumley's (1973) observation that drag reduction is characterized by the displacement of a 'Newtonian core flow' (Warholic et al. 1999).

In the experimental studies different kind of measurement instrument have been used to observe the drag reduction. The oldest instrument is Hot-wire Anemometer (Virk et al. 1967); it was used for the turbulent intensities and energy spectrum measurements and it is an unreliable technique because experiments are conducted by inserting wire into the flow system. The other one is Particle- Image Velocimetry (PIV) (Warholic et al. 2001), which was used to observe strange turbulent fields that occurred when drag reduction was quite large, but measurements with PIV did not provide enough photographs to obtain precise statistics. Photon Correlation Spectroscopy (PCS) (Van Dam et al. 1994, Bhat et al. 2000), although PCS measures

the instantaneous Lagrangian velocity difference over a distance and obtains spatial information on the distribution of the small velocity differences, relative to the mean flow, it does not measures time dependent flow velocity. Real-time hologram interferometer (Achia and Thompson 1977); this technique aimed obtaining pictures of the wall region during the drag reduction. Flow visualization techniques are restricted due to the flow cross sections of relatively small effective diameter and low polymer concentration. To improve resolution and to provide a means of quantitative analysis, the refractive index of the wall layer is enhanced. The most common measurement instrument is Laser Doppler Velocimetry (LDV) (Wei and Willmarth 1992, Sá Pereira and Pinho 1994, Gyr and Tsinober 1997, Den Toonder et al. 1997, Ptasinski et al. 2001); LDV measures the velocity component which is perpendicular to the axis of the light beam. LDV measures the velocity of a single particle, so that to obtain a velocity profile is not easy. Additionally, LDV can not be applied to the system when the liquid is non transparent and contains too many particles (Signal-Processing).

In this study, drag reduction effect of CMC at concentrations lower than 1000 wppm on turbulent pipe flow is investigated. Ultrasound Doppler Velocimetry (UDV) which is a non-invasive and non-destructive and relatively new technique is employed in the flow measurements. UDV provides velocity profile in seconds (Signal-Processing). Its relatively low cost and ease of use are other considerable advantages on the other aforementioned measurement techniques. The results of this study are also compared with the available drag reduction models in the literature.

CHAPTER 2

DRAG REDUCTION

In this chapter, details of the drag reduction are provided. First experimental methodologies used and the results reported in the literature are introduced. The drag reduction mechanisms proposed in the literature are also included.

2.1 The Onset of Drag Reduction (Onset Hypothesis)

The Onset Hypothesis, reported by Virk et al. (1967), predicts the starting point of drag reduction phenomenon with respect to molecular weight of polymer and inside diameter of pipes used in the experiments. This hypothesis explains the relation between macromolecular diameter and dissipative turbulence scale at onset. The effective diameter, D_M, of a random coiling macromolecule in dilute solution is about twice its rms radius of gyration, R_G, independent of concentration.

Drag reduction as an energetic phenomenon and the rates of dissipation and production of turbulent energy are known to show sharp maxima at $y^+ \approx 10$; y^+ being the usual dimensionless distance from the wall. Therefore, the parameter chosen to characterize the turbulence was a 'dissipation wave-number', k_d, derived from a turbulent energy spectrum close to the wall.

The onset of drag reduction in the turbulent flow of dilute polymer solutions occurs at a constant value of the product $D_M k_d^*$ which is a ratio of the dimensions of the macromolecule and the fine scale of the turbulent shear flow (Virk et al. 1967).

Besides, the onset of drag reduction occurs at a rather well defined onset wall shear stress. For a given polymer solution it is essentially the same in pipes of different diameters. For a given polymer solvent combination, the onset wall shear stress is independent of polymer concentration, and onset depends on the polymer random coil size in solution, with the onset wall shear stress increasing as radius of gyration decreases (Virk, 1975).

Lumley (1969) suggested the time criterion hypothesis to explain this phenomenon. Drag reduction occurs when the relaxation time is longer than the time scale of turbulent eddy.

According to the viscoelastic models (Min et al. 2003) drag reduction exists when,

$$We_{\tau} > \alpha \,, \tag{1}$$

where We_{τ} is the Weissenberg number (ratio of the relaxation time to the time scale of the near wall turbulence) normalized by the friction velocity and α depends on the viscoelastic model. The variation of drag with the Weissenberg number was showed and seen that the drag reduction occurs at We>1 and We>0.3, respectively, for Re=3000 and 15000 and the drag decreases more with larger Weissenberg number.

After the onset of drag reduction adding larger amount of polymer to the system decreases the drag, but at a certain concentration it does not change, this point is termed as Maximum Drag Reduction asymptote (MDR) and discovered by Virk et al. in 1967. It is independent of pipe diameter and strikingly insensitive to polymer species, molecular weight, and concentration. An asymptotic regime of maximum possible drag reduction in which the friction factor relation is insensitive to the polymer solution employed, being, universally (Virk, 1975),

$$\frac{1}{\sqrt{f}} = 19.0 \log \sqrt{f} - 32.4 \tag{2}$$

Maximum drag reduction mechanism studied by Min et al. (2003), using direct numerical simulation. An Oldroyd-B model is adopted to express the polymer stress because MDR is closely related to the elasticity of the polymer solution. This model shows good agreement with Virk's MDR asymptote.

For small drag reduction, the rms streamwise velocity fluctuations decrease in the viscous sublayer but increase in the buffer and log layers with increasing Weissenberg number, *We*, but they decrease in the whole channel and nearly zero near the wall for large drag reduction. The production of turbulent kinetic energy decreased with increasing *We*, because of the decreasing Reynolds shear stress, but the polymer returned more energy from the elastic energy to turbulence, preventing the disappearance of turbulence. Therefore, the noticeable effect of polymer additives at the state of MDR was turbulence generation as well as drag reduction (Min et al. 2003).

2.2. Drag Reduction Visualization and Measurement

The extent of drag reduction is determined by pressure drop measurements. But to understand the mechanisms involved, the effect of the presence of the macromolecules on the turbulent flow structure should be investigated. This is accomplished by flow measurements which mainly include both instantaneous and time-average velocity profile, turbulent kinetic energy distribution. For this purpose number of different velocity measurement techniques have been employed. The most common one is Laser Doppler Velocimetry (LDV) (Wei and Willmarth 1992, Sá Pereira and Pinho 1994, Gyr and Tsinober 1997, Den Toonder et al. 1997, Ptasinski et al. 2001). The others are Hot-wire Anemometer (Virk et al. 1967), Particle- Image Velocimetry (PIV) (Warholic et al. 2001), Photon Correlation Spectroscopy (PCS) (Van Dam et al. 1994) and real-time hologram interferometer (Achia and Thompson, 1977).

For carrying out measurements of turbulence-velocity fluctuations with the Hot-wire Anemometer, two different methods are applied. In the first method the electric current is kept constant; in the second method the temperature and so the electric resistance is kept constant (Hinze, 1959). A constant temperature anemometer with cylindrical, quartz coated, hot film sensors were used for turbulent intensity and energy spectrum measurements by Virk et al. (1967).

In the literature, measurements of turbulence have been done mostly using Laser Doppler Velocimetry (LDV) technique. LDV measures the instantaneous velocity. System uses the two orthogonal pairs of laser beams. The velocity at the intersection point of the beams is obtained through the processing of the light originating from the measurement point. This method enables fast, accurate velocity measurements. It is, on the other hand, is suited for single point velocity per measurement and for transparent materials (Den Toonder et al. 1997).

Particle-image velocimetry (PIV) was used to study the effect of drag-reducing polymers on the structure of turbulence by Warholic et al. (2001). The principle of operation is that the images of the particles in a light sheet are captured on a film. The light sheet is double-pulsed so that two images of each particle are obtained. The distance between them divided by the time interval gives the velocity of the particle in the plane of the light.

The real-time hologram interferometry (visualization technique) was used to provide detail of the wall region during drag reduction by Achia and Thompson (1977). The flow patterns in the wall region were made visible by infusing a refractive-index enhancer into the flow. Phase variations in the flowing stream due to the enhancer introduced upstream of the observation field were visualized and recorded as real-time distortions of an interference fringe system. These fringe movements provided information on turbulence in the wall layer.

The photon correlation spectroscopy (PCS) technique was used by Van Dam et al. (1994). PCS technique measures the instantaneous Lagrangian velocity difference

over a distance and this dynamic light scattering technique is very suitable for measurements on the turbulence, since one obtains information on the distribution of the small velocity differences, relative to the mean flow.

2.3 Experimental Parameters in Drag Reduction Studies

2.3.1 Effects of Polymer Concentration

For low concentrations the drag reduction is found to be directly proportional to the concentration, for high concentrations the reduction reaches to a maximum designated as the maximum drag reduction (MDR) asymptote (Lumley, 1969). To observe the effect of polymer concentration an experimental study was carried out in the same pipe for solutions of the same polymer with different concentrations. Friction factor versus Reynolds number plots at different polymer concentrations occur in a region confined between an upper limit Prandtl-Karman law and MDR curve. It is seen that the drag reduction effect of polymer additive increases with increasing polymer concentration (Wójs, 1993, Sá Pereira and Pinho, 1994).

2.3.2 Effects of Polymer Molecular Weight

Molecular weight of the polymer strongly influences the effectiveness of the polymer in reducing drag. As the molecular weight is increased the onset of drag reduction occurs at lower Reynolds number (Virk, 1975). Smaller amounts of high molecular weight polymer can interact with a liquid in turbulent flow to decrease the drag, so that lower concentrations are required to perform the same drag reduction level compared to the low molecular weight polymers.

Zakin and Hunston (1980) reported the drag reduction effect of molecular weight distribution of polystyrene in toluene. The molecular weights (M_W) of polystyrene sample were 7.1×10^6, 4.1×10^6 and 2.4×10^6. The results showed that the drag reduction is affected by the molecular weight distribution of polymer. High M_W enables higher drag reduction. For example, at the same polymer concentration (100 wppm) and experimental conditions, polystyrene solution with 7.1×10^6 molecular weight causes 63% drag reduction while those of 4.1×10^6 and 2.4×10^6 molecular weights are 42% and 18%, respectively.

It is known that the high molecular weight polymer chains in polymer solutions can be subjected to degradation (chain scission) and lose their effectiveness for a time. Liberatore et al. (2004) observed that initial drag reduction levels decreased over the course of experiments in which they used aqueous polyacrylamide solutions.

2.3.3 Effects of Pipe Diameter

Pipe diameter is another important parameter in drag reduction. Virk (1975) reported that the onset of drag reduction shifts toward higher polymer concentrations with increasing pipe diameter. In their study Gasljevic et al. (1999) found that drag reduction of a polymer solution becomes more pronounced as pipe diameter is reduced. It has been speculated that dependence of the drag reduction characteristics on pipe diameter is due to the changing length scale ratio of the polymer chains to turbulence. As diameter increases, larger eddies is observed which suppresses the drag reduction ability of the polymer.

2.4 Comparison of Polymeric and Surfactant Additives

Cationic, anionic, and zwitterionic surfactants are used as drag reducer additives in the turbulent flow and the researches on these have grown in recent years. The drag reducer additives are generally used recirculation turbulent flow system, therefore investigations focus on the additives which do not degrade or repair themselves after degradation.

The differences in the flow behaviors of polymeric and cationic surfactants were studied by Myska and Zakin (1997). According to this study, polymer solutions degrade irreversibly when sheared and lose their drag reduction behavior. Cationic surfactants degrade under high shear, but the structures are repairable and they regain their drag reducing ability when shear is reduced. Dilute polymer solutions become drag reducing when the critical shear rate exceeded. Surfactant solutions generally show a gradual departure from the laminar flow curve and drag reducing until a critical shear rate is reached. Friction factors significantly below those predicted by the maximum drag reduction asymptote for high polymers can be reached in cationic surfactant and aluminum disoap systems. Turbulent mean velocity profiles for cationic surfactants can be significantly steeper than the limit predicted by the elastic sublayer model for the high polymers (Myska and Zakin, 1997).

Despite their higher level drag reductions than polymers, use of surfactants has been quite limited. The main drawback of surfactants is on their negative impact environment compared to polymers.

2.5 Flow Quantities and Turbulence Measurements

The basic quantities measured for this experimental study are volumetric flow rate, pressure drop and the velocity profiles. The Reynolds number used in the calculations is defined as given below,

$$\mathrm{Re} = \frac{D < V > \rho}{\mu} \tag{3}$$

The average velocity of the flow is calculated by using volumetric flow rate data of the flow and given by,

$$< V >= \frac{Q}{\pi R^2} \tag{4}$$

The pressure drop values though the pipe is obtained by using the equation given as,

$$\Delta P = g\Delta h\left(\rho_m - \rho_{s,p}\right) \tag{5}$$

For a fully developed turbulent flow, the mean stress at the wall is given,

$$\tau_w = \frac{D}{4}\frac{\Delta P}{\Delta x} \tag{6}$$

The Fanning friction factor can be written,

$$f = \frac{\tau_w}{\frac{1}{2}\rho < V >^2} \tag{7}$$

The amount of drag reduction, DR, is expressed as the wall shear stress difference between the solvent (water), τ_s, and the polymer solutions, τ_p, at the same Reynolds number,

$$DR\% = \frac{(\tau_s - \tau_p)}{\tau_s} \times 100 \tag{8}$$

In fully developed pipe flow, dilute polymer solutions exhibit three distinct regimes which are, in order of increasing flow rate (Virk, 1975):

1. A regime without drag reduction in which the friction factor relation is the same as for solvent, that is, the usual Prandtl-Karman law,

$$\frac{1}{\sqrt{f}} = 4.0 \log(\mathrm{Re}\sqrt{f}) - 0.4 \tag{9}$$

2. A regime with drag reduction in which the friction factor relation depends upon the nature of the polymer solution and an approximate relation for this regime is,

$$\frac{1}{\sqrt{f}} = (4.0 + \delta) \log(\mathrm{Re}\sqrt{f}) - 0.4 - \delta \log\sqrt{2}\, d\, W^* \tag{10}$$

where δ, W^* are polymer solution parameters.

3. An asymptote regime of maximum possible drag reduction in which the friction factor relation is insensitive to the solution employed, universally,

$$\frac{1}{\sqrt{f}} = 19.0 \log(\mathrm{Re}\sqrt{f}) - 32.4 \tag{11}$$

The friction velocity,

$$U^* = \sqrt{\frac{\tau_w}{\rho}} \tag{12}$$

and non-dimensional velocity distance is,

$$u^+ = \frac{\bar{U}}{U^*} \tag{13}$$

where $\bar{U}$ is time average velocity and non-dimensional radial distance is,

$$y^+ = \frac{U^* y \rho}{\mu} \tag{14}$$

The turbulent boundary layer is divided into the three parts: the viscous sublayer very near the wall

$$u^+ = y^+ \qquad y^+ < 5 \tag{15}$$

The other one is the logarithmic (inertial) sublayer,

$$u^+ = 2.5 \ln y^+ + 5.5 \qquad y^+ > 30 \tag{16}$$

Eqn. (16) is called the Prandtl-Karman law (universal logarithmic velocity distribution). The region between the logarithmic sublayer and the viscous sublayer is called buffer sublayer, where

$$5 < y^+ < 30 \tag{17}$$

The root mean square (rms) of the velocity fluctuations in the axial direction,

$$u'_{rms} = \sqrt{\overline{u'^2}} \tag{18}$$

The dimensionless form of the Eqn. (18) is,

$$u'^{+}_{rms} = \frac{\sqrt{\overline{u'^2}}}{U^*} \tag{19}$$

Eddy viscosity data are derived from velocity profile and flow measurements. Total shear stress calculated using the pressure drop measurements is,

$$\tau = \tau_v + \tau_t \tag{20}$$

where τ total local shear stress, τ_v is the viscous shear stress and τ_t is the turbulent shear stress.

$$\tau = (\mu + \varepsilon)\frac{d\bar{U}}{dr} \tag{21}$$

Eqn. (21) is denoted as Boussinesq relation where μ is the dynamic viscosity of the solution and ε is the Eddy viscosity, by this way Eddy viscosity values are calculated at each radial position.

2.6 Mechanisms

2.6.1 Lumley Theory

Lumley (1969, 1973), explained the mechanism of the drag reduction as 'Molecular Extension'. The coiled polymer chains stretch, if the strain rates of turbulence are large enough, outside the viscous sublayer. This situation increases the effective (extensional) viscosity in the turbulent flow region, but the viscosity near the wall in the viscous sublayer remains lower. The higher effective viscosity in turn increases the viscous sublayer thickness which leads to drag reduction. The onset of drag reduction occurs when the relaxation time of the polymer is longer than the time scale of turbulence.

Lumley suggested that the drag reduction originates from the increase of local effective viscosity, but did not give the detailed experimental results and theoretical models supporting the mechanism. Therefore, Hinch (1977), proposed polymer elongation models to show the elongation of polymer molecule results in an increase of the effective viscosity theoretically. Besides, Landahl (1977), applied two-scale model to analyze the mechanism and found that the anisotropic stress caused by the extension of the polymeric coils leads to drag reduction. Ryskin (1987) constructed a quantitative theory of drag reduction, using the Yo-Yo model to predict the viscosity increase in the turbulence.

2.6.2 Hinch Theory

The extended state of randomly coiled macromolecules was investigated by Hinch (1977) and four models were considered which show the importance of the inextensibility of the polymer chain and the variation of the friction coefficient with

the extension. The first model is ‘Elastic ellipsoid model’ explaining the dependence of the stretching by bulk flow on the distortion. The main features of this model are, the frictional grip of the flow increases with the distortion so that the large distortions can be maintained by some weak flows so long as the initial distortion is large enough and in strong flows the distortion will grow until it is limited by the finite extensibility of the polymer chain. The second model is ‘Inextensible flexible thread model’ considering the effect of hydrodynamic stretching and inextensibility. An inextensible flexible thread straightens starting from the S shape. Firstly, the thread tends to an orientation in which it is in tension and then this tension snaps the thread straight. The third model is ‘Transversely diffusing thread model’. According to this model weak motions acting on a straight thread cause small transverse distortions which can be described by a diffusion process in the deformation space. There is less transverse displacement at the center compared to the ends of the thread due to the high degree of tension. Associated with the transverse distortions is a small coiling effect; the ends of the inextensible thread must come closer when the thread is not straight. The shortening varies as the small strength of the weak motion. Flow strength needed to maintain the stretched polymer is weaker than the flow required producing the initial large distortion of the random coil. This result simply reflects the increased frictional grip on the polymer. The last one is ‘Elastic rod model’. Here relatively straight polymer can respond much slower or much faster than the relaxation time of the randomly coiled polymer. If the flow is strong, then in equilibrium the polymer is virtually fully expanded, hard against the stops of the nonlinear springs. The polymer then responds very quickly and often almost as a rigid rod. At large distortions the polymer relaxes slowly against the large frictional resistance. After a short time the polymers are fully extended and in a regime where the nonlinear elasticity produces a fast response to changes. Under this condition polymer solution behaves much the same as a suspension of rigid rods which have high viscous resistance to any extensional motion in the direction of the rods and a low resistance to other motions (a high extensional viscosity with a low shear viscosity). This anisotropy of the suspension influences the structure of flows which are combinations of straining and shear. The high extensional viscosity in strong flows is the principle instrument in reducing drag.

2.6.3 Landahl Theory

Landahl (1977), applied 'Two-Scale Model' to investigate the dynamics of boundary layer turbulence and the mechanism of drag reduction. In order to analyze the effect of localized turbulence production on a large scale field, a two-scale model was proposed in which the small scale motion produced by secondary inflectional instability was considered as the driving mechanism for the large-scale one through the creation of localized Reynolds stresses resulting from the small-scale mixing. On the basis of the model proposed the phenomenon of turbulent drag reduction due to the additives of various kinds appears most easily explained as being caused by stabilization of the inflectional velocity profiles due to the additive.

2.6.4 Yo-Yo Theory

This model was introduced by Ryskin (1987), and the conical channel system of a dilute polymer solution is investigated theoretically. The stress field due to the polymer additives is calculated using a new molecular model based on the physical picture of the polymer molecules unraveling in strong flows. Yo-yo model states that macromolecules elongate under straining action of flow. That introduces additional elongation viscosity which increases thickness of the viscous sublayer or decrease in the drag. The model capture large polymer effect during the transient deformation of a macromolecule by the extensional flow and extensional viscosity increases in turbulence due to the straightening macromolecules.

According to Lumley, Hinch, Landahl and Ryskin, the main source of the drag reduction is the increase in the local effective viscosity of the flow due to hydrodynamic interaction between polymer chains and flow. In their study, elastic effect of dilute polymer solutions was not considered. Thus, De Gennes (1986)

investigated the energy exchange between the kinetic and elastic energy in the core of the turbulent flow, far from the boundary.

2.6.5 De Gennes Theory

De Gennes (1986), proposed a different model in which the polymer effects at small length scales were explained by 'elastic modulus.' This model suggests the elasticity responsible from the drag reduction. Flexible polymers in dilute solutions enhance the viscosity in slow flows. At each distance y from the wall, there is a cascade and it is truncated elastically. This gives a law for the minimum eddy size r^{**} versus distance y. But in strong, rapidly varying shear fields, they behave elastically. A turbulent cascade (from large to small scales) should thus be deeply modified when the elastic stresses become comparable to the Reynolds stress. The main idea of this model is that the flexible coils in the dilute regime, behave elastically at high frequencies. A Kolmogorov cascade remains unaltered by polymer additives only down to a certain limit r^{**} where the polymer stresses balance the Reynolds stresses. In some cases this occurs at full stretching and the viscous effects may be dominant.

Drag reduction effects of polymer additives have been studies in a number of studies in pipe flows using homogeneous (a well mixed solution of polymers) polymer solution. And to answer the question as to whether or not polymer drag reduction is a phenomenon taking place exclusively near the wall region, Bewersdorff et al. (1993) investigated local turbulent properties affected by the injection of concentrated polymer solutions into certain regions in the pipe.

2.6.6 Bewersdorff et al. Theory

The heterogeneous drag reduction was first reported in 1970s. The concentrated polymer solutions are injected into the core-region of a turbulent pipe or channel flow, it is seen that high level of drag reduction can be obtained by injection of polymer solution into a turbulent pipe flow (Bewersdorff et al. 1993).

The experiments indicate that the injection location affects strongly the drag reduction. In rectangular channel three different positions equally spaced from each other and from the walls were obtained. It was seen that drag reduction with one injection point is extremely low in comparison to the three injection points at the same average polymer concentration. For one injector the lower observed drag reduction could be explained by the fact that the l/d (in where l is the down stream distance from injector and d is the pipe or hydraulic diameter) in the spanwise direction is not sufficient to reach the asymptotic value of drag reduction in the entire section. For two and three injectors the spanwise distance from one injector to the wall and to the center of the channel is identical. Therefore, no change in drag reduction should occur if dissolved molecules are the source of the observed drag reduction. This is consistent with the view that the thread coming out of the injection tip interacts directly with the large scale structures in its region of influence. In homogeneous drag reduction, it is assumed that the active polymer in the buffer layer responsible for the drag reduction. Thus, one should expect a decrease in drag reduction when water is injected through the wall; however this expectation is not supported by the experimental results.

The experimental results suggest two main effects related to the heterogeneous drag reduction; small amount of polymer is transferred from the thread and to the bulk fluid, the resulting effect seems to be conceptionally similar to the drag reduction in dilute homogeneous drag reduction. The other result is that the viscoelastic thread can interact with the bulk of the flow. Consequently, the heterogeneous drag reduction is in part caused by small amount of dissolved polymer in the near-wall

region as well as by an interaction with the turbulence. The mechanism of this interaction is still not clear, but it is speculated that this should be a kind of self-induced forcing leading to suppressing of the Reynolds stress and this forcing can be realized via a region in the core flow.

CHAPTER 3

ULTRASOUND DOPPLER VELOCIMETRY

Ultrasound Doppler technique was originally applied in the medical field and dates back more than 30 years. The use of pulsed emissions has extended this technique to other fields and has opened the way to new measuring techniques in fluid dynamics. The term "Doppler ultrasound velocimetry" implies that the velocity is measured by finding the Doppler frequency in the received signal, as it is the case in Laser Doppler velocimetry. In fact, in ultrasonic pulsed Doppler velocimetry, this is never the case. Velocities are derived from shifts in positions between pulses which results in the same effect on the received signal as the Doppler shift. This is explained in the next part (DOP 2000 User's Manual).

3.1 Doppler Effect

The Doppler effect is the change in frequency of an acoustic or electromagnetic wave resulting from the movement of either the emitter or receptor. Consider an ultrasonic transducer which emits waves of frequency f_e and remains fixed in a medium where the speed of sound is given by c. A receptor or a target given in Figure 3.1.1 moves with a velocity v. By convention, v is considered negative when the target is moving toward the transducer. If the trajectory of the target forms an angle Θ_1 with respect to the direction of propagation direction of the ultrasonic wave, the frequency of the waves perceived by the target, f_t, will be,

$$f_t = f_e - \frac{f_e v \cos\Theta_1}{c} \tag{22}$$

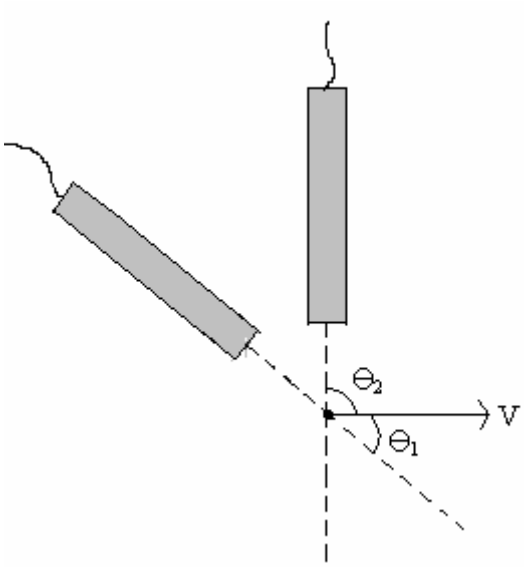

Figure 3.1.1 The Positions of Ultrasonic Probes.

If the acoustic impedance of the target is different from that of the surrounding medium, the waves will be partially reflected. The target acts as a moving source of ultrasonic signals. The frequency of the waves reflected by the target, f_r, as measured by a stationary receiver is,

$$f_r = f_e + \frac{f_e v \cos\Theta_2}{c} \tag{23}$$

As the velocity of the target is much smaller than the speed of sound ($v<<c$) it is reasonable to neglect the second order terms. The difference between the emitted and received signals, which is known as the Doppler frequency shift, f_d, is then expressed by,

$$f_d = \frac{f_e v(\cos\Theta_1 - \cos\Theta_2)}{c} \tag{24}$$

If the same transducer is used for receiving the signals the above equation becomes,

$$f_d = \frac{2 f_e v \cos\Theta_1}{c} \tag{25}$$

3.2 Pulsed Doppler Ultrasound

In pulsed Doppler ultrasound, instead of emitting continuous ultrasonic waves, an emitter sends periodically a short ultrasonic burst and a receiver collects continuously echoes issues from targets that may be present in the path of the ultrasonic beam. By sampling the incoming echoes at the same time relative to the emission of the bursts, the shift of positions of scatterers are measured. Assume a situation, as illustrated in Figure 3.2.1, where only one particle is present along the ultrasonic beam.

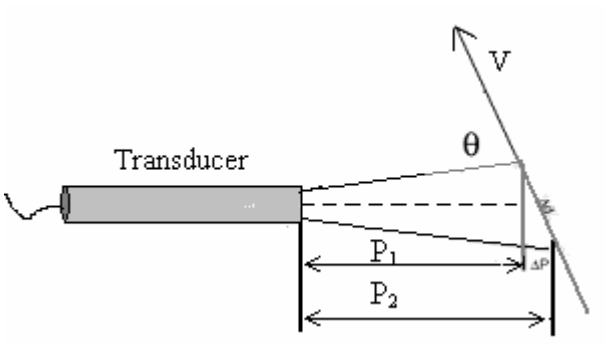

Figure 3.2.1 The Path of the Ultrasonic Beam.

From the knowledge of the time delay, T_d, between an emitted burst and the echo issue from the particle, the depth, P, of this particle can be computed by,

$$P = \frac{cT_d}{2} \tag{26}$$

If the particle is moving at an angle Θ regarding the axis of the ultrasonic beam, its velocity can be measured by computing the variation of its depth between two emissions separated in time by T_{prf},

$$\left(P_2 - P_1\right) = vT_{prf}\cos\Theta = \frac{c}{2}\left(T_2 - T_1\right) \tag{27}$$

The time difference (T_2-T_1) is always very short, most of the time lower than a microsecond. It is advantageous to replace this time measurement by a measurement of the phase shift, δ, of the received echo. This phase shift is defined by the following relation,

$$\delta = 2\pi f_e\left(T_2 - T_1\right) \tag{28}$$

With this information the velocity of the target is expressed by,

$$v = \frac{c\delta}{2f_e\cos\Theta T_{prf}} = \frac{cf_d}{2f_e\cos\Theta} \tag{29}$$

The last equation gives the same result as the Doppler equation. But one should always be aware that the phenomena involved are not the same. Assume that the particles are randomly distributed inside the ultrasonic beam. The echoes issues from each particle are then combined together in a random fashion, giving a random echo signal. Hopefully, a high degree of correlation exists between different emissions (DOP 2000 User's Manual).

3.3 Advantages and Limitations

The main advantage of pulsed Doppler ultrasound is its capability to offer spatial information associated to velocity values. Unfortunately, as the information is available only periodically, this technique suffers from the Nyquist theorem. This means that a maximum velocity (V_{max}) exists for each pulse repetition frequency,

$$V_{\max} = \frac{c}{4(2) f_e \cos\Theta T_{prf}} \tag{30}$$

In addition to the velocity limitation, there is a limitation in depth. The ultrasonic burst travels in the liquid at a velocity which depends on the physical properties of the liquid. The pulse repetition frequency gives the maximum time allowed to the burst to travel to the particle and back to the transducer. This gives a maximum depth (P_{max}) of,

$$P_{\max} = \frac{T_{prf} c}{2} \tag{31}$$

From the above two equations, it is seen that increasing the time between pulses (T_{prf}) will increase the maximum measurable depth, but will also reduce the maximum velocity which can be measured. The maximum velocity and maximum depth are thus related according to the following equation,

$$P_{\max} V_{\max} = \frac{c^2}{8 f_e} \tag{32}$$

At any given instant, an echo signal come from many different depths, corresponding to echoes from previously emitted signals. The presence of several acoustic interfaces also causes several reflections which can cause a false determination of the target depth. Nevertheless, if PRF is sufficiently low (a few kHz), the attenuation of

previously emitted pulses will render them indiscernible. The same goes for reflected signals. With a large increase in the PRF, pulsed Doppler ultrasound can approach the properties of continuous wave Doppler, with a loss of axial resolution but no maximum velocity limitation. Other important advantages of UDV include non-invasive measurements and applicability to both opaque and transparent media (Signal-Processing).

3.4 Operation of the Velocimeter

The investigated liquid must contain particles to receive echo from the solution at sufficient level. The size of the particles must be smaller than the wave length in order to avoid any diffraction of the ultrasonic beam. This is often the case and most of liquid contains enough very small gas bubbles, dust or impurities. In addition, particles are also added solutions when necessary.

The ultrasonic probe can be placed directly in contact with the liquid or coupled to the wall of the container by means of an ultrasonic gel. The coupling medium provides good contact with the wall and reduces the refraction of the sound.

One of the most important parameter is the choice of the ultrasonic probe. This choice is generally based on; the velocity range, the depth resolution and the attenuation of the ultrasonic wave (Signal-Processing).

CHAPTER 4

EXPERIMENTAL

4.1 Flow System

The experiments were carried out using a recirculation flow system which is shown in Figure 4.1.1. The flow system consists of test section which is 6 m polyvinylchloride (PVC) tubing with 46 mm inner diameter, connection plastic tubing, an in-line flow meter, valves, two plastic tanks and a pump (Iwaki Magnet Pump, Japan). The straight tubing upstream of the UDV probe is sufficient to ensure fully developed flow ($L/D \approx 110$). A constant water head is maintained by pumping the solution from the lower tank to the upper one. Both the overflow from the upper tank and the return flow from experimental section are received in the lower tank. The constant head allowed operation at a steady average flow rate. In UDV measurements large pipe diameters ensure higher number of measurements points of the velocity profile giving higher spatial resolutions compared to smaller diameter. In addition large diameters enable to obtain higher number of velocity data near the wall, which is especially critical in turbulent flow regimes. 46 mm pipe diameter resulted in satisfactory velocity measurements which were performed using UDV system of Signal-Processing.

The pressure drop measurements were taken over a 6 m long PVC pipe with a length of 1.0 m provided from the entry (to avoid the entry problems) and 1.0 m from the exit by a U tube manometer with $CHCl_3$ (Chloroform). The length between the pressure tap is 4 m.

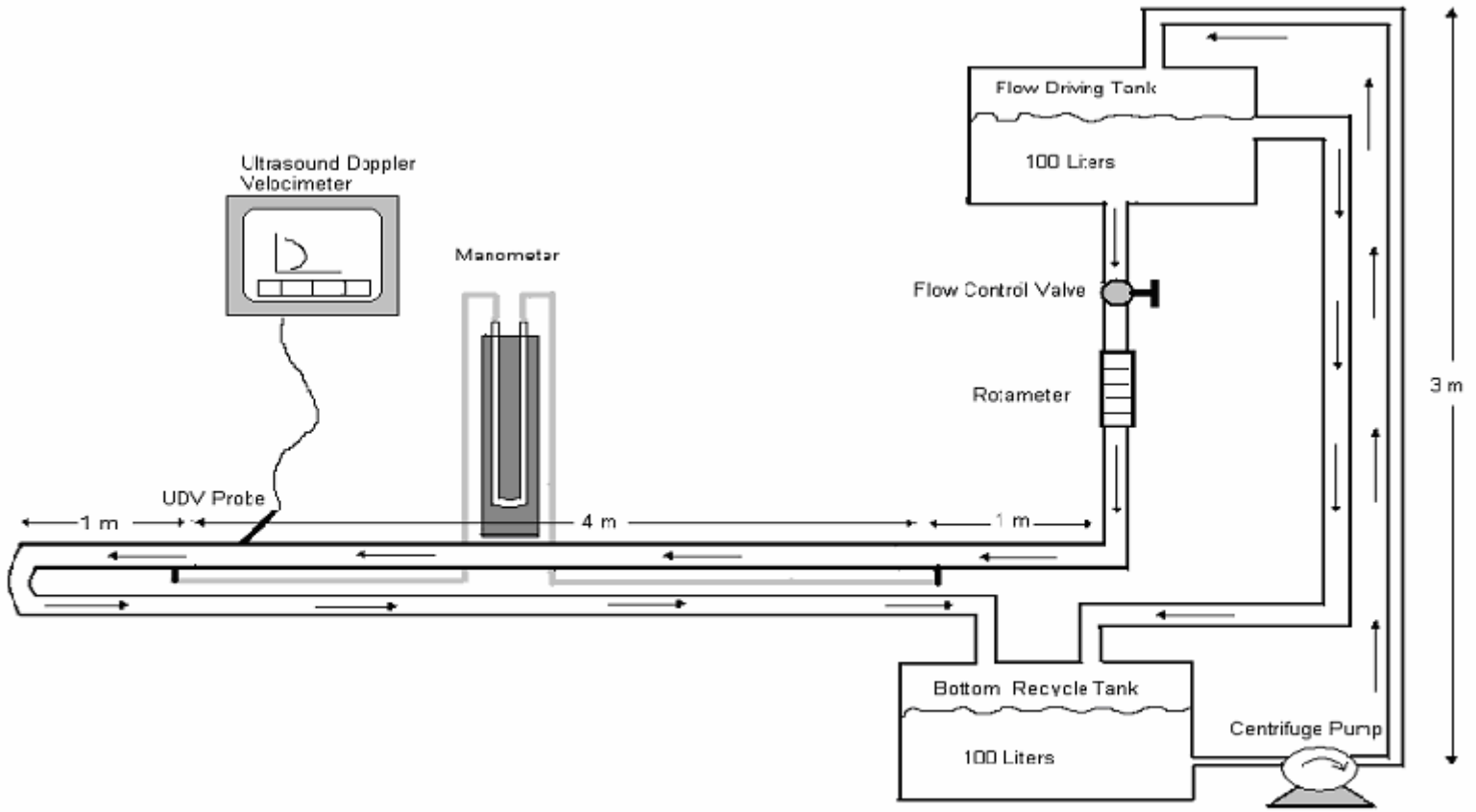

Figure 4.1.1 Experimental Set-up

4.2 Preparation of Polymer Solutions

Experiments were carried out with aqueous solutions of the Sodium Carboxymethylcellulose (CMC) supplied by SIGMA Chemical Company. Properties of CMC is given in Table 4.2.1. CMC was chosen because of its low molecular weight, so that the mechanical degradation effect can be eliminated during the circulation of the solution.

Table 4.2.1 Properties of Sodium Carboxymethylcellulose

Molecular Weight	Viscosity of a %1 aqueous solution	Sodium Content	Purity	Appearance
700 kDa	1500 to 3000 cp	8%	99.5%	White to yellow with an orange cast powder

For the experimental study, polymers were dissolved in tap water. First, the tanks were filled with 138 liter water. An amount of 28 g CMC was dissolved in two liter water and the solution was stirred for two hours using a stirring vessel (Servodyne Mixer, Cole-Palmer). Then the concentrated CMC solution was added to the tanks so that 200 wppm CMC solution was obtained. Other concentrations (300, 400, 500 wppm) were prepared by adding CMC to this solution. Before the experiments, polymer solutions were allowed to stand 12 hours at room temperature and during this time the covers of tank were closed to prevent the evaporation.

4.3 Flow Conditions

The experiments were performed using pure solvent (water) and solutions at four different CMC concentrations (200, 300, 400, 500 wppm). Volumetric flow rate range was in between 0.313 L/s and 0.909 L/s corresponding to the Reynolds number range of 5000 to 20000. Before the experiments the solutions were characterized by density (calculated from mass and volume measurements) and viscosity (HAAKE Viscotester VT-01, Germany) measurements at room temperature. The results are given in Table 4.3.1.

Table 4.3.1 Physical properties of solutions at room temperature.

	Water	200 wppm	300 wppm	400 wppm	500 wppm
ρ, kg/m^3	980	983	983	985	985
μ, Pa.s	1×10^{-3}	1.2×10^{-3}	1.35×10^{-3}	1.65×10^{-3}	1.8×10^{-3}

Then, the desired flow rate was established in the pipe using the flow control valve and the rotameter. Velocity profile measurements were done using the UDV system. Pressure drop was also recorded simultaneously by means of the manometer. The experimental data were then processed to obtain non-dimensional velocity profiles, turbulent intensities, eddy viscosities. Drag reduction levels were obtained through the pressure drop measurements.

4.4 Velocity Profile Measurements

Velocity profiles were obtained using UDV which measures the velocity component in the direction of the ultrasonic beam and the UDV system used in this study is shown in Figure 4.4.1.

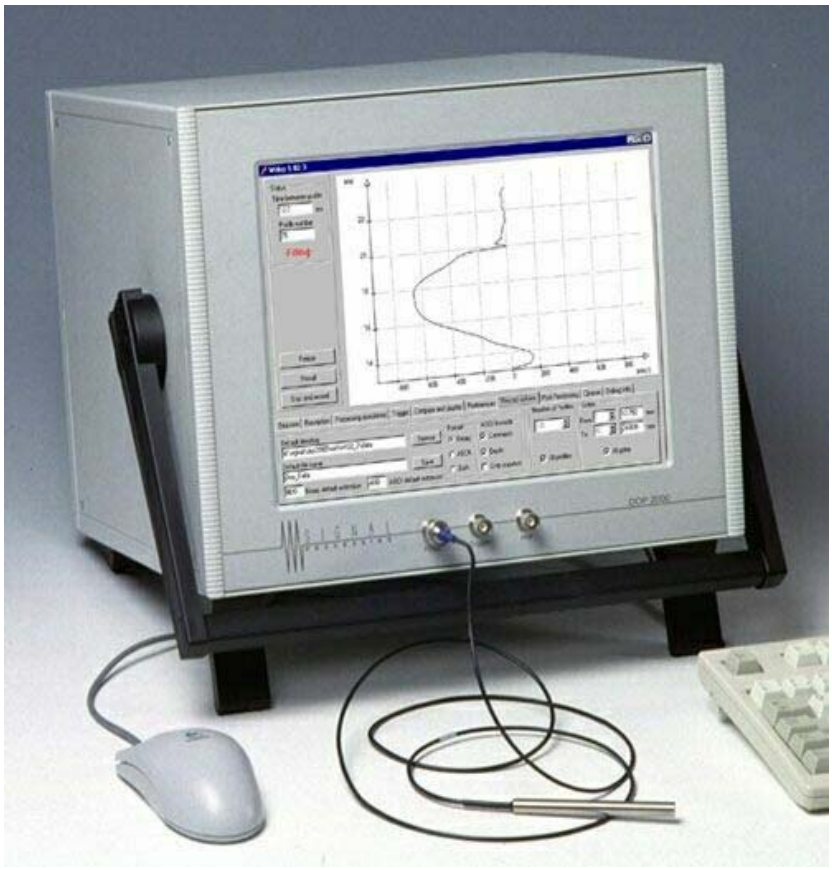

Figure 4.4.1 Ultrasound Doppler Velocimeter.

Presence of tiny particles or scatterrers, help to improve signal to noise ration of the measurements. Thus 12 g Griltex 2A P1 copolyamide particles (EMS-Griltech,

Switzerland) were added to the solution. Having average diameter of 3 micron in liquid, particles did not lead to any appreciable diffraction of the ultrasonic beam with wavelength 372.5×10^{-6} m around 3 micron.

A container was designed to place the ultrasonic probe on the PVC pipe and it was filled with coupling liquid (water) to reduce refraction of the ultrasonic waves. This container is depicted in Figure 4.4.2.

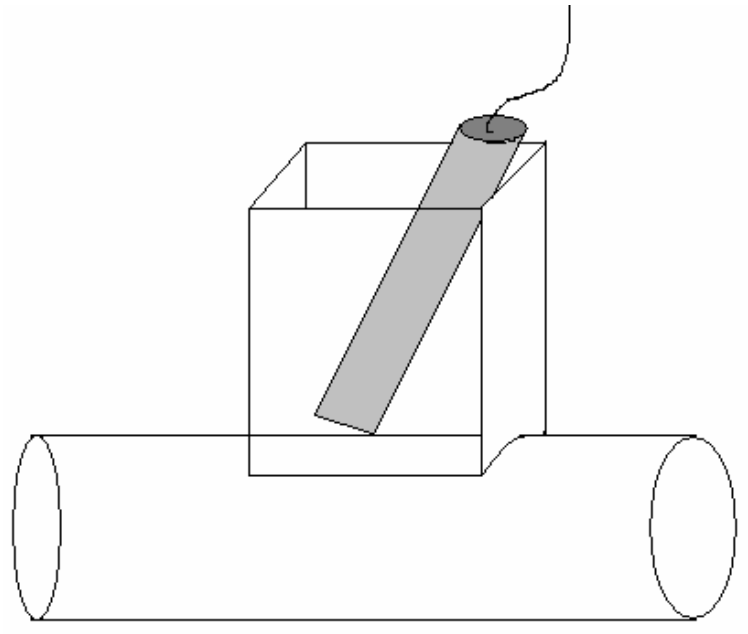

Figure 4.4.2 Container Filled with Water for the Ultrasonic Probe.

The angle between the ultrasonic probe and pipe was 70 degree. The ultrasonic probe (TR0405LS) which was used for the experiments has 4 MHz frequency with 5 mm diameter and 90 mm length. UDV parameters employed in the experiments are given in Appendix B.

4.5 UDV Parameters

In this part details of the UDV measurements parameters are provided.

Pulse repetition frequency (PRF): The pulse repetition frequency determines the maximum measurable depth as well as the maximum Doppler frequency which can be measured unambiguously. The maximum depth is simply given by the half of the distance covered by the ultrasonic burst when it travels in the medium during a time equal to the time between two emissions. As the PRF is nothing else than the sampling rate of the ultrasonic echo, the Nyquist limit defines the maximum Doppler frequency shift that can be measured unambiguously. Therefore the PRF defines the maximum velocity for a given emitting frequency. As a consequence, both limits, the maximum velocity and the maximum depth, are linked together through Eqn. (32). In the UDV system used in this study, the value of the pulse repetition frequency may be chosen between 15.625 Hz or 64μs and 100 Hz or 10000 μs by increment of 1μs.

Resolution: The DOP2000 defines the resolution as the distance between the center of adjacent sampling volumes and not the thickness of the sampling volume. The UDV system has 6 different bandwith values, covering a range from 50 kHz to 300 kHz. This defines a longitudinal dimension of the sampling volume from about 0.64 mm to 3.19 mm in water.

Sensitivity: The algorithm used to measure the Doppler frequency computes the mean frequency of the Doppler spectrum. When the Doppler energy decreases, the mean value become more and more random due to the noise included in the spectrum. In order to avoid the apparition of random values of the screen, the DOP2000 computes also the level of Doppler energy received and allows the user to cancel the computation of the Doppler frequency if the level of the Doppler energy is below a user's defined value. The sensitivity parameter contains 5 different values, which define the level below which the computation is cancelled.

Emitting power: The emitted ultrasonic power has to be selected in order to receive enough backscattered energy from the particles and to avoid as much as possible saturation in the receiver stage of the DOP2000. A high emitting power induces more ringing in the transducer and more dissipated energy. The level of emitting power was low in the experiments.

Definition of the amplification level (TGC): Correct values of the amplification level are important. A high level may induce saturation in the receiver stage of the DOP2000, which induces wrong measurement values. The amplification level was approximately 50dB in the measurements.

4.6 The Speed of Sound

The knowledge of the speed of sound in the medium is necessary to transform the Doppler frequency shifts to velocity, and the time of flight of the ultrasonic waves to the radial position. The sound speed measuring unit given in Figure 4.6.1 allows to measure the sound speed in a liquid by measuring the precision time that is taken by an ultrasonic burst to propagate over a defined distance. Typical value of the sound speed in the solutions was 1490 m/s.

Figure 4.6.1 Sound Speed Measuring Unit

CHAPTER 5

RESULTS AND DISCUSSION

In this chapter the results obtained from pressure drop measurements and Ultrasound Doppler Velocimeter (UDV) measurement are presented. The results are compared with the literature qualitatively.

5.1 Pressure Drop Measurements

In the experiments drag reduction was determined by pressure drop measurements in fully developed turbulent pipe flow along the pipe. Volumetric flow rate measurements were used to obtain bulk average velocity as defined in Eqn. (4). Pressure drop values were converted to the friction factor through Eqns. (6) and (7). This procedure is repeated at each polymer concentration and flow rate. Plots of the friction factor versus Reynolds number obtained at different polymer concentrations are shown in Figure 5.1.1. The graph shows the level of drag reduction for each polymer solutions.

At each polymer concentration friction factor decreases as Re gets higher and then it becomes constant with respect to Re. Since there is no drag reduction in laminar flow, friction factors at different polymer concentration converge to the same value as Re decreases.

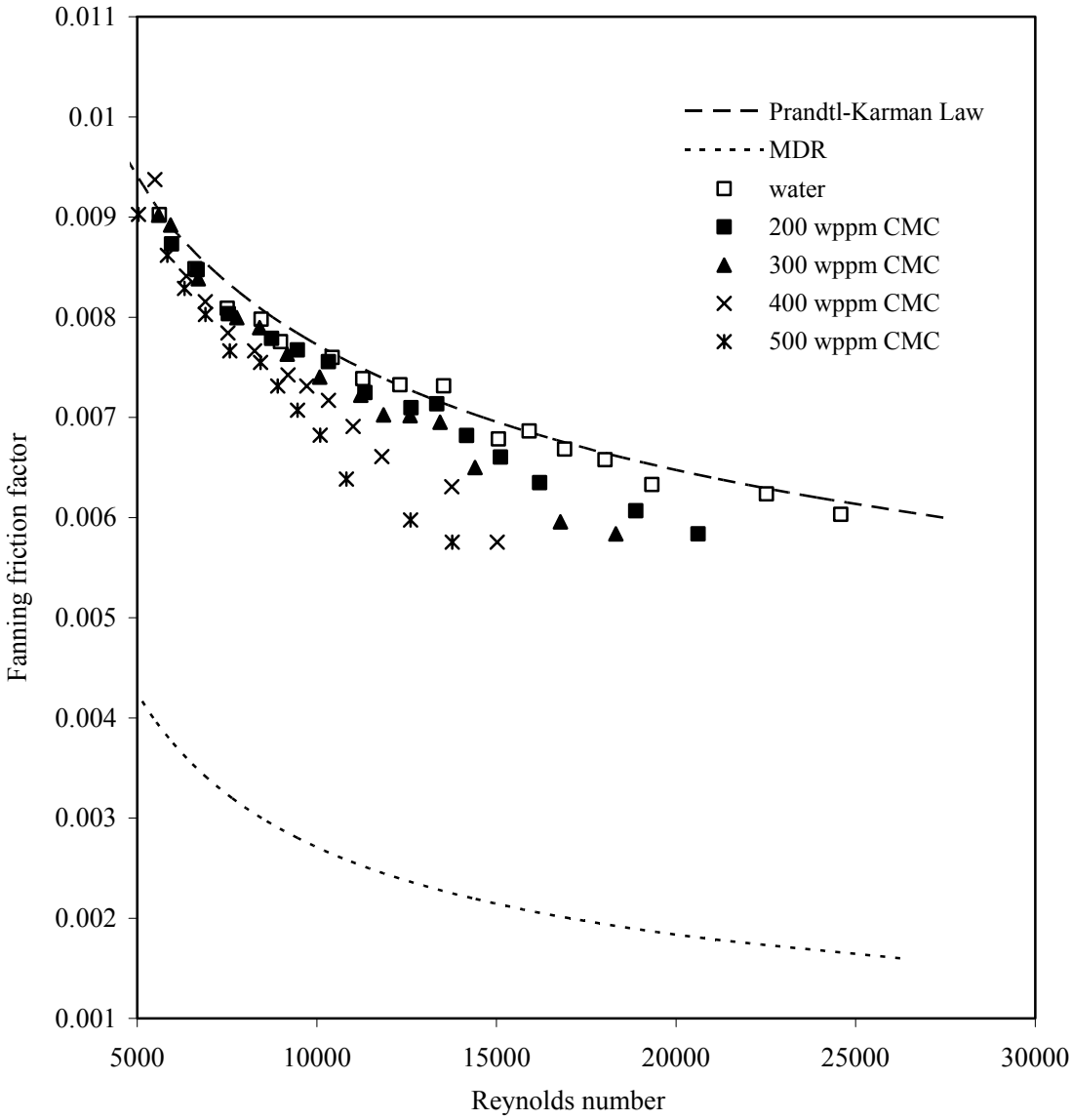

Figure 5.1.1 Fanning Friction Factor versus Reynolds Number.

The effect of polymer concentration on the drag reduction appears in the form of lower friction factor at any Re value. In the figure it is obvious that high polymer concentration yields higher drag reduction and that becomes more and more pronounced in highly turbulent flows.

Also included in Figure 5.1.1 are Prandtl-Karman law (the law of the wall) and MDR curves. The data for the water are good agreement with the Prandtl-Karman law, which is the upper line. The law of the wall is one of the famous empirically-determined relationships in turbulent flow near solid boundaries. Measurements show that, for both internal and external flows, the streamwise velocity in the flow near the wall varies logarithmically with distance from the surface (Wilcox, 1998).

MDR asymptote was defined by Virk et al. (1967) and it was seen that after the onset of drag reduction, the addition of polymer increases drag reduction until a certain value called as MDR asymptote. Once that level of drag reduction is reached, further addition of polymer has no impact on drag reduction. Theoretical derivation of MDR was given by Virk et al. (1967) and also experimental studies were performed to attain this asymptote. The results showed that MDR asymptote is insensitive to polymer species, molecular weight, concentration and pipe diameter. A satisfactory explanation of mechanism for the existence of MDR asymptote for drag reduction is still lacking.

Pinho and Whitelaw (1990) used four concentrations (1000, 2000, 3000 and 4000 wppm) of Carboxymethylcellulose in pipe flow. They observed MDR at 2000 wppm CMC solution. In this study, the concentrations of CMC solutions used are not high enough to reach MDR asymptote. Our primary objective was to investigate drag reduction itself. In order to avoid possible complications associated with the high polymer concentrations around MDR, 500 wppm was chosen the maximum CMC concentration in the experiments.

The effect of Reynolds number for each polymer solution on drag reduction is given in Figure 5.1.2. Drag reductions were obtained using Eqn (8) where τ_s is the wall shear stress for water at a certain Re number and it was calculated using the pressure drop data; τ_p is the polymer wall shear stress calculated using friction factor, f_p, was determined using Figure 5.1.1 at the same Re value of f_s. Figure 5.1.2 depicts higher drag reductions are achieved when the polymer concentration is increased. Drag

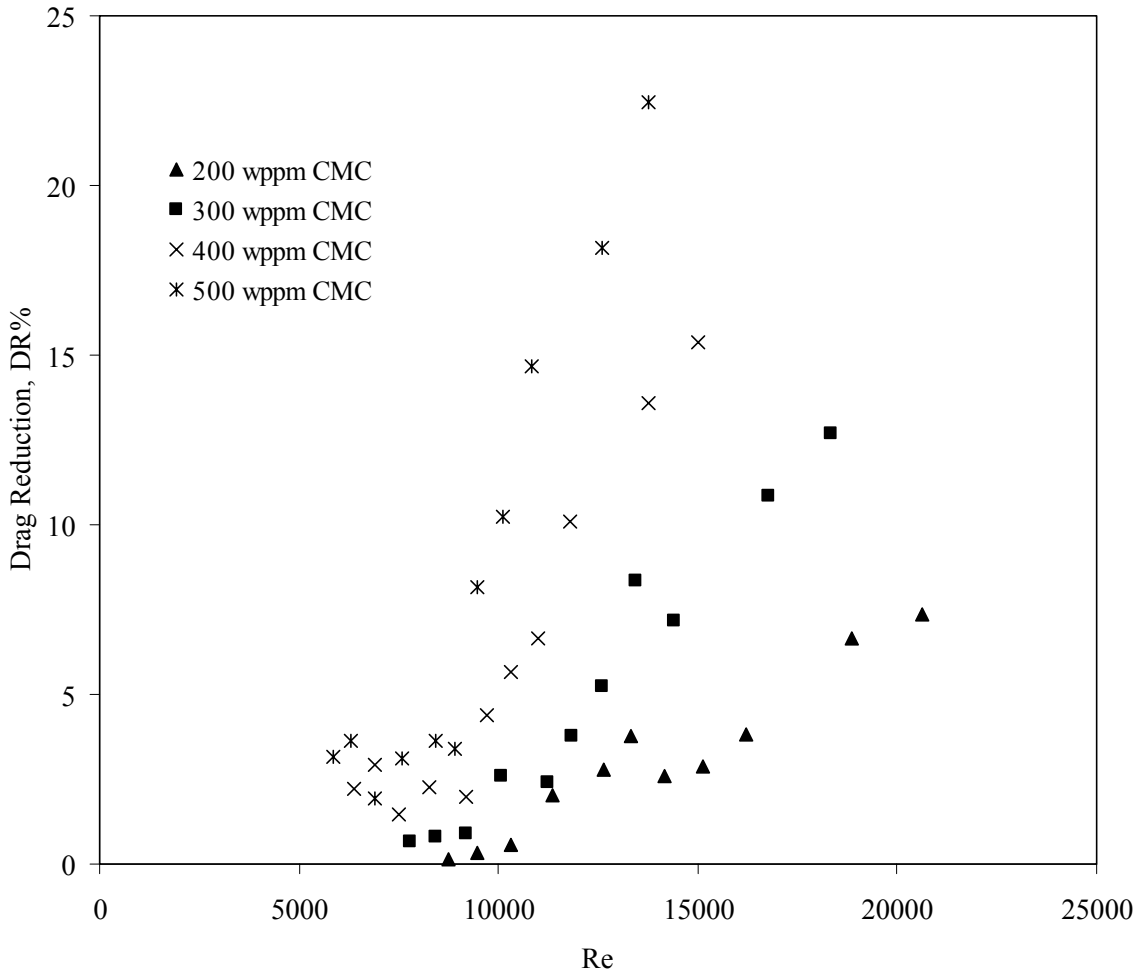

Figure 5.1.2 Drag Reduction versus Reynolds Number of Various Concentrations of CMC Solutions

reduction becomes further higher at high Re numbers. In the experiments maximum drag reduction achieved was 22 % using 500 wppm CMC solution, which is a considerable value compared to those reported in literature. For example Pinho and Whitelaw (1990) reported 46.8 % drag

reduction at 1000 wppm CMC solution at Re number 17000. It should be noted that both the concentration and Re values were higher than the values used in this study so that higher drag reduction was observed in the reported study.

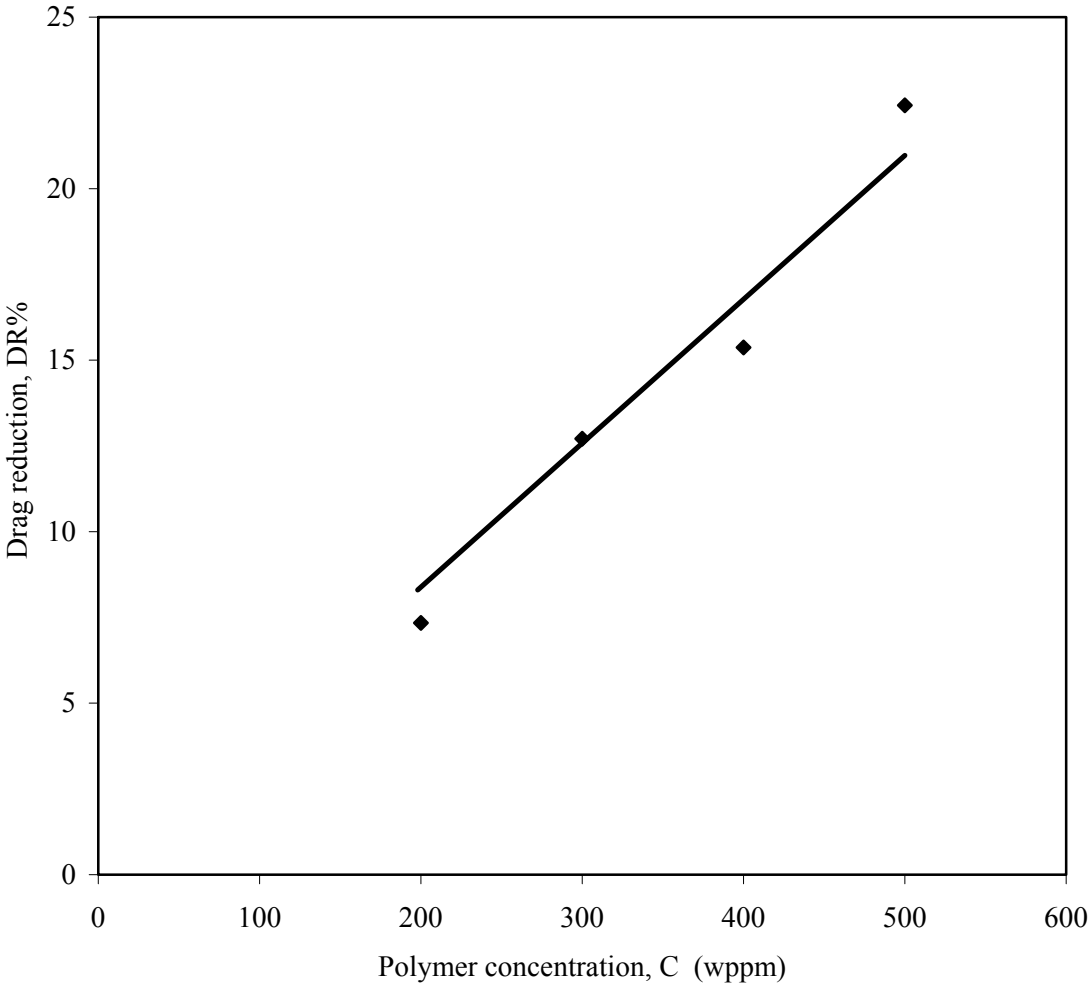

Figure 5.1.3 Drag Reduction versus Polymer Concentration.

Figure 5.1.3 shows the drag reduction values with respect to CMC concentration at the same bulk average velocity, <V>, of 0.55 m/s. As expected drag reduction increases by the addition of polymer to the solution. That increase can be approximated by a linear relation within the studied range of CMC concentration as shown in the figure. The drag reductions versus polymer concentration characteristics are consistent with results of Pinho and Whitelaw (1990) and Escuider et al. (1999).

The results obtained so far clearly demonstrate that higher drag reductions can be attained as polymer concentration and flow rate, hence Re, are increased. The results, on the other hand, do not provide any direct clue to the mechanisms of drag reduction. To answer the question "how does drag reduction occur" the impact of polymer addition on the turbulent flow field should be determined. Therefore in this study a new flow measurement technique, UDV, was used to obtain both time-averaged and fluctuating velocity distributions within the pipe simultaneously with the pressure drops. The flow measurement results are included in the following section.

5.2 Velocity Profiles Measurements

Velocity profiles obtained at different polymer concentrations using UDV are depicted in Figure 5.2.1. Vertical axis normalized time-averaged velocity while the horizontal axis is normalized radial position. The time average velocity data at the center of the pipe, $\bar{U}_o$, and pipe radius R were used to scale the velocity and position, respectively. In the figure all velocity profiles exhibit typical characteristics of time-averaged velocity distribution in a turbulent flow. Little velocity variation in the core and a high velocity gradient near the wall are observed. Addition of polymer has small impact on the core region while it decreases the velocity gradient near the wall appreciably. Therefore highest gradient is observed in the case of water flow without polymer. It decreases with increasing polymer concentration. It is well known that degree of momentum interaction between the wall and flow is directly dependent on that gradient. Hence lower velocity gradient in the case of flow with polymer gives rise to lower shear stress or drag.

According to Lumley, the only difference in the boundary layer turbulence structure between the Newtonian flows and the drag reducing flows is that polymer molecules are expanded in the flow outside the viscous sublayer due to possible stretching of the polymer molecule, this causes an increase in the effective viscosity, which in turn

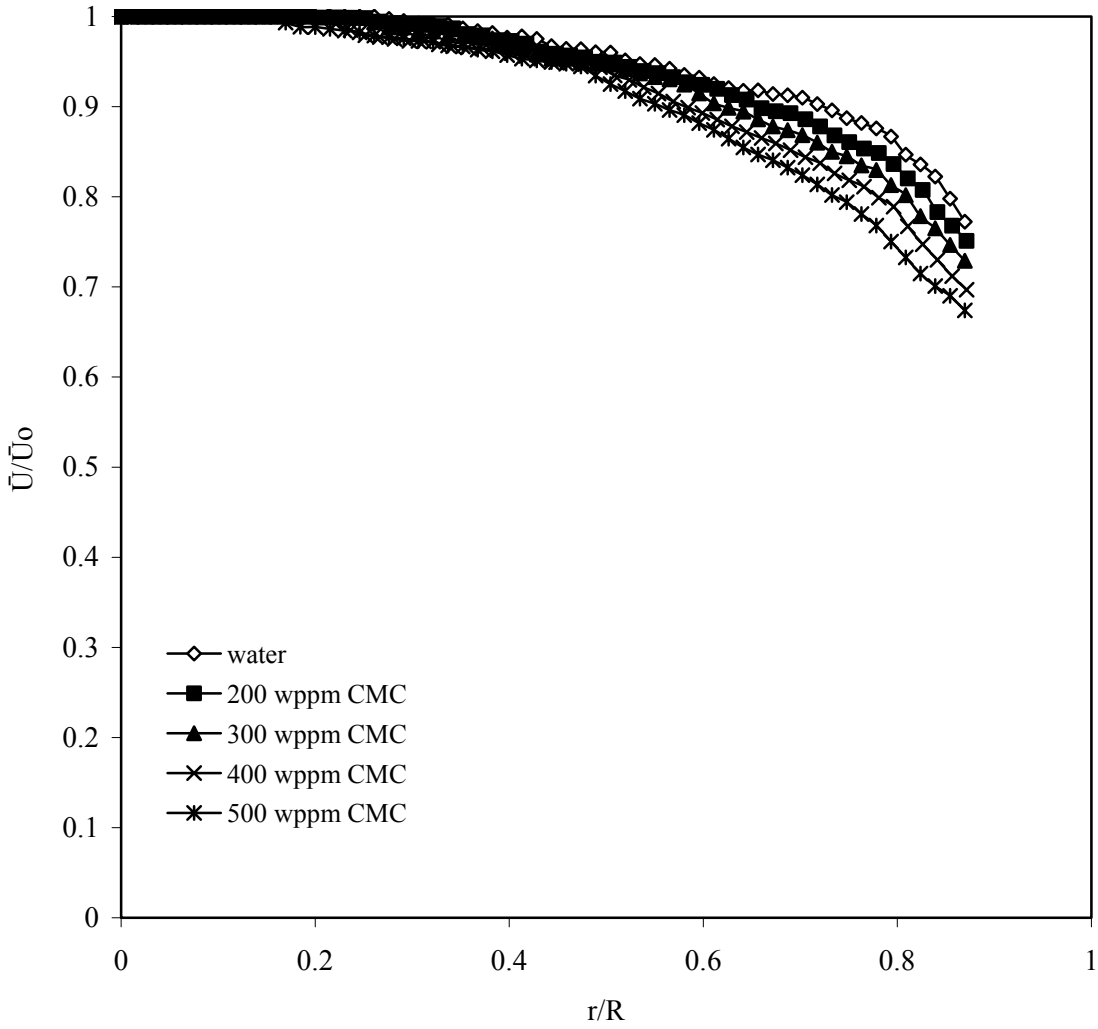

Figure 5.2.1 Mean Axial Velocity Profiles of Water and Various Concentration of CMC Solutions.

damps dissipative eddies. This effectively leads to a thickening of the viscous sublayer leading to a decrease in the velocity gradient at the wall. The observed decrease in the velocity gradient at high polymer concentrations in Figure 5.2.1 also indicates the thickening of the viscous sublayer.

The closest velocity measurement to the wall was achieved at 3 mm from the wall. This distance corresponds to the logarithmic sublayer under the flow conditions of the experiments. Due to the resolution limitations and negative interactions with the pipe wall velocity data could not been obtained in the regions closer the wall where viscous sublayer occurs. Unfortunately important hydrodynamic interactions between turbulent flow and the solid surfaces are mostly confined to this region. Nevertheless the results obtained in the outer regions have many crucial implications regarding to the turbulence and drag reduction characteristics as reported below.

De Gennes (1986) suggested that the decrease of the velocity gradient near the pipe wall by adding polymer is because of elasticity. When the polymer is added to the flow system, polymer absorbs the turbulent kinetic energy near the pipe wall and transforms it to the elastic energy. After that, the fluid particles containing the elastic energy stored near the wall are lift up by the near-wall vertical motion and the elastic energy is released into turbulent kinetic energy or dissipated in the buffer and logarithmic layer. Thus, the polymer actively intervenes in the energy transfer.

Therefore, in order to obtain drag reduction, the relaxation time of the polymer should be long enough (longer than turbulent time scales) to transport the elastic energy from the near wall region to the buffer and logarithmic layer (Min et al., 2003). This theory is supported by the heterogeneous drag reduction experiment in which the polymers are injected in the center of the pipe (Warholic et al., 2001). These authors establish that in these cases drag reduction is a wall effect localized in the buffer layer.

To observe the behavior of polymer in the turbulent boundary layer, the typical velocity profile for turbulent boundary layer has to be shown. In Figure 5.2.2 the universal non-dimensional mean velocity profiles are plotted as a function of non-dimensional radial distance from the wall. Velocities are non-dimensionalised using friction velocity given in Eqn. (12). This figure also includes several velocity curves; Prandtl-Karman Law (the Newtonian wall law) profile, the viscous sublayer profile and MDR. The velocity data at low values of y^+ could not be obtained, therefore the

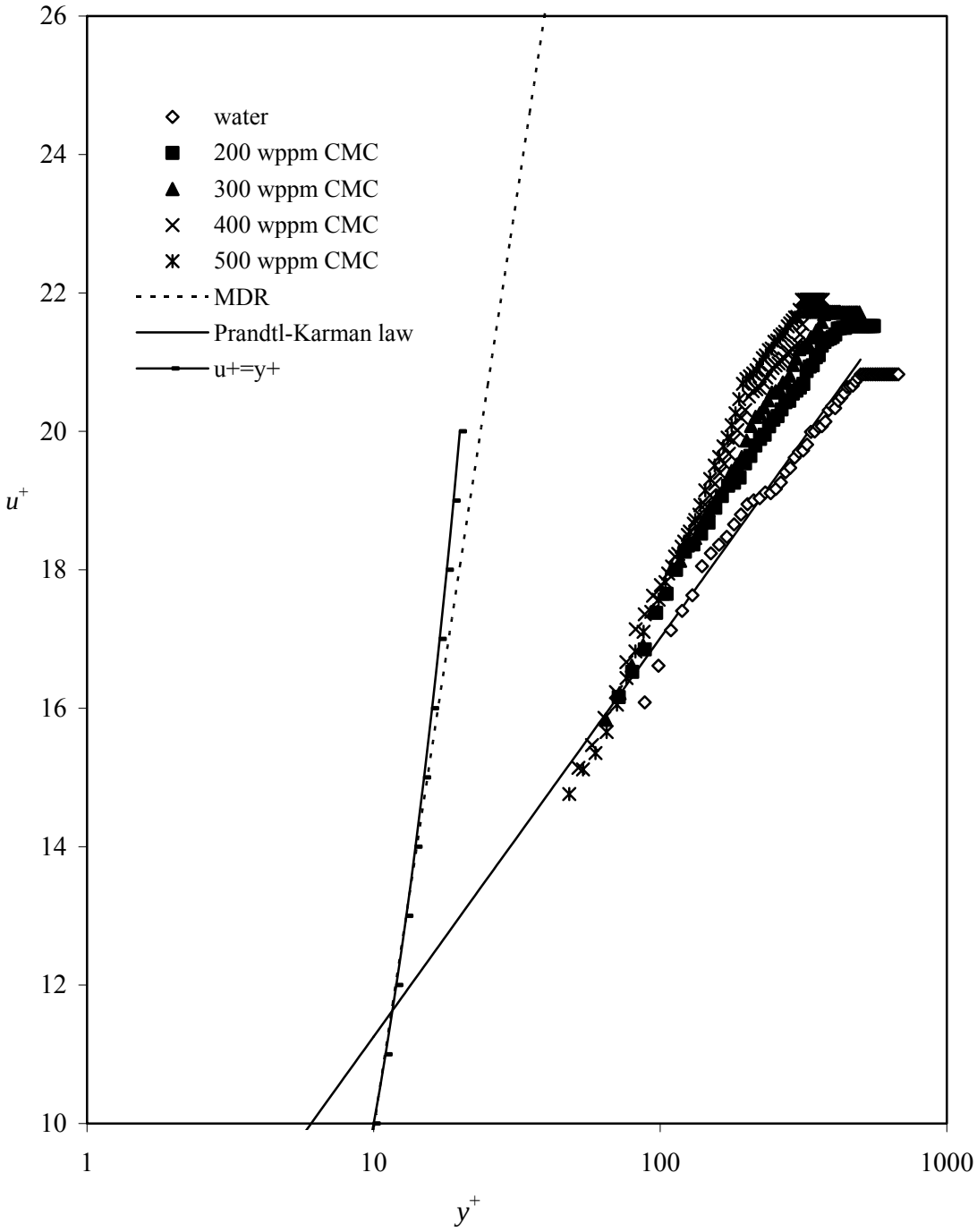

Figure 5.2.2 Mean Axial Velocity Profiles of Water and Various Concentration of CMC Solutions in Terms of Wall Units.

comparison between the results of this study and literature can not be done in the viscous and buffer sublayer. In Figure 5.2.2 the slope of the profiles increases with polymer concentration since high polymer concentrations yield lower wall shear stresses hence lower friction velocities which are used to scale the velocities in the figure. According to Den Toonder et al. (1997) the buffer layer is thickened due to polymer additives and this causes an upward shift of logarithmic profile.

The effect of CMC addition on the logarithmic layer is investigated by obtaining turbulence intensities using UDV data. Time-dependent velocity fluctuations are obtained by using Eqn. (18) and the axial root-mean-square velocity fluctuations, u'_{rms}, are calculated. The variation of the axial root-mean-square velocity fluctuation with the dimensionless radial distance from the pipe centre is shown in Figure 5.2.3. Turbulent intensities show the characteristic behavior for the drag reduced flow. For polymer concentrations, with the exception of 200 wppm CMC, the height of the peak increases with respect to water and the peak shift away from the wall for 300, 400 and 500 wppm CMC solutions to a lower r/R value. These findings are consistent with the results of Warholic et al. (2001) and Den Toonder et al. (1997) qualitatively.

The height of the peak increases with addition of polymer. This sudden increase shows that the turbulent energy of the axial velocity near the wall is transported from small scales to the large scales. The change is the largest when r/R value is 0.9, this point corresponds to logarithmic sublayer. This result is consistent with the shift of the logarithmic sublayer in the axial mean velocity profile. Therefore, it is seen that, polymers suppress the turbulence by decreasing its energy near the pipe wall.

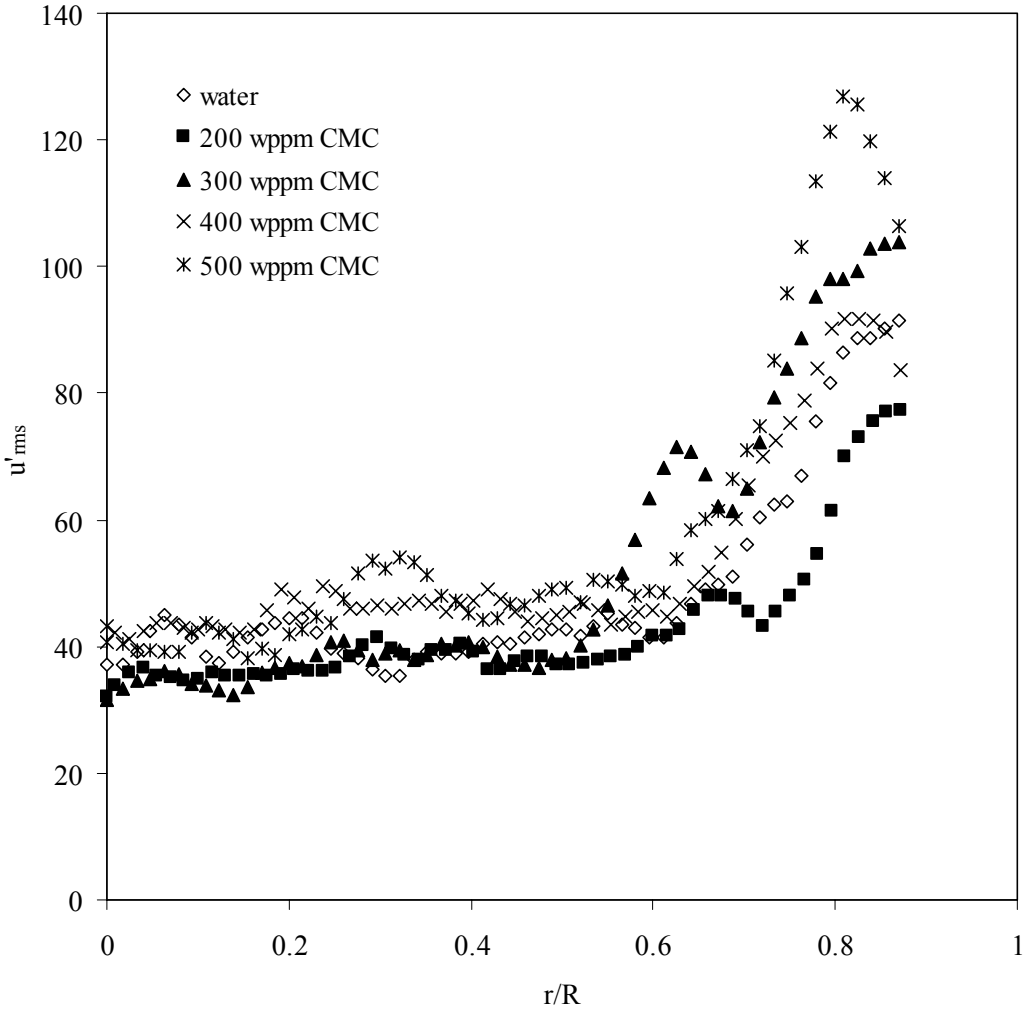

Figure 5.2.3 Mean Axial Turbulence Intensity Profiles for Water and CMC Solutions.

Eddy viscosity profiles during the drag reduction are given in Figure 5.2.4. They were derived from velocity profile and flow measurements. The eddy viscosity through the pipe radius decreases by adding polymer. Near the pipe wall it takes the lowest value. This finding is consistent with Virk's study (1975). Figure 5.2.4 shows that, turbulence property of the flow is diminished by polymer and this leads to suppressed turbulence. Drag reduction phenomenon suggests that polymer solutions undergoing turbulent flow in a pipe require a lower pressure drop to maintain the

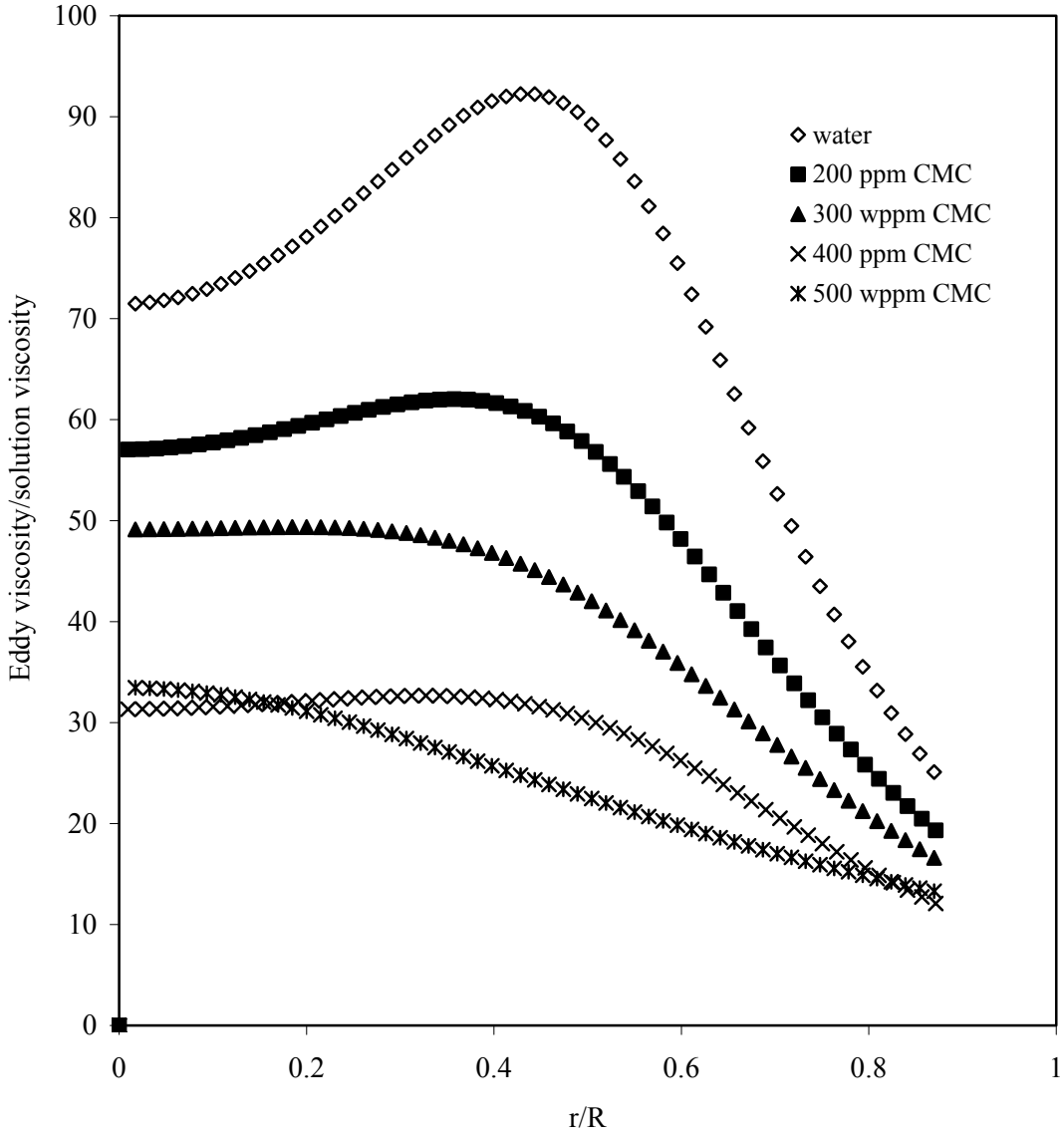

Figure 5.2.4 Non-dimensional Eddy Viscosity Profiles for Water and CMC Solutions.

same volumetric flow rate. Consequently, a larger volumetric flow rate can be obtained at the same pressure drop when polymer additives are introduced. The energy of the turbulence is used to increase the flow rate.

CHAPTER 6

CONCLUSIONS

In this study drag reduction in fully developed turbulent pipe flow with four concentrations (200 to 500 wppm) of low molecular weight Sodium Carboxymethylcellulose (CMC) in aqueous solutions was investigated experimentally. Drag reduction was determined through pressure drop measurements. In order to observe the impact of the presence of the polymer on the flow, Ultrasound Doppler Velocimetry (UDV) was employed to monitor the instantaneous velocity distributions.

The graph of friction factor versus Reynolds number shows the level of drag reduction for each polymer solutions. The data for the water are good agreement with the Prandtl-Karman law. The effect of polymer concentration on the drag reduction appears in the form lower friction factor at any Re value. High polymer concentration yields higher drag reduction and that becomes more pronounced in highly turbulent flows.

Higher drag reductions are achieved when the polymer concentration is increased and there is an approximately linear relation within the studied range of CMC concentration. In the experiments maximum drag reduction achieved was 22 % using 500 wppm CMC solution.

All velocity profiles obtained using UDV exhibit typical characteristics of time-averaged velocity distribution in a turbulent flow. Addition of polymer has small impact on the core region while it decreases the velocity gradient near the wall appreciably. The highest gradient is observed in the case of water flow. It decreases

with increasing polymer concentration. Lower velocity gradient in the case of flow with polymer gives rise to lower shear stress or drag.

Velocity data could be obtained as close as 3 mm to the wall by UDV due to the limitations and negative interactions with the pipe wall. It is known that, important hydrodynamic interactions between turbulent flow and the solid surfaces are mostly confined to this region. Therefore, an exact result about the behavior of polymer in viscous sublayer and buffer sublayer explaining the drag reduction mechanism can not be suggested.

The behavior of polymer in the turbulent boundary layer is obtained. The slope of the profiles increases with polymer concentration since high polymer concentrations yield lower wall shear stresses hence lower friction velocities.

Turbulent intensities show the characteristic behavior for the drag reduced flow. For polymer concentrations, with the exception of 200 wppm CMC, the height of the peak increases with respect to water and the peak shift away from the wall for 300, 400 and 500 wppm CMC solutions to a lower r/R value. This increase shows that the turbulent energy of the axial velocity near the wall is transported from small scales to the large scales. The change is the largest in logarithmic sublayer. This result is consistent with the shift of the logarithmic sublayer in the axial mean velocity profile. Therefore, it is seen that, polymers suppress the turbulence by decreasing its energy near the pipe wall. Radial and tangential root-mean-square velocity fluctuations could not be obtained by UDV.

The eddy viscosity through the pipe radius decreases by adding polymer. Near the pipe wall it takes the lowest value. Turbulence property of the flow is diminished by polymer and this leads to suppressed turbulence.

As a result, polymer molecules are stretched at a point near the wall and below this point turbulence is suppressed and after that turbulence takes higher value. These results are consistent with the literature qualitatively.

RECOMMENDATIONS

The turbulence measurements near the wall for 46 mm inside diameter pipe using Ultrasound Doppler Velocimetry is very difficult, but UDV gives very reliable velocity data in the turbulent core region and measurements can be done easily in a short time. Drag reduction behavior of polymer additives should be examined with the larger inside diameter pipe or rotational apparatus with large diameter using UDV, therefore velocity data very close to the wall can be obtained.

UDV technique may be improved to obtain radial and tangential root-mean-square velocity fluctuations therefore the effects of CMC on turbulent flow field can be observed certainly.

The results of this experimental study may be tested by a model and a sensible mechanism can be suggested.

The Ultrasound Doppler Velocimetry is a developing technique and opens the way to the new measuring techniques in fluid dynamics. Studies to improve this technique are going on.

REFERENCES

Achia, B.U., and Thompson, D.W., *Structure of the Turbulent Boundary in Drag-Reducing Pipe Flow*, J. Fluid Mech., 81, pp. 439-464, 1977.

Bewersdorff, H.W., Gyr, A., Hoyer, K., and Tsinober, A., *An Investigation of Possible Mechanisms of Heterogeneous Drag Reduction in Pipe and Channel Flows*, Rheologica Acta, 32, pp. 140-149, 1993.

Bhat, S.K.P., Pal, K., Chopra, S., *A Study of Intermittency and Drag Reduction in Turbulence by Dynamic Laser Light Scattering*, Experiments in Fluids, 28, pp. 160-164, 2000.

De Gennes, P.G., *Towards A Scaling Theory of Drag Reduction*, Physica, 140A, pp. 9-25, 1986.

Den Toonder, J.M.J., Hulsen, M.A., Kuiken , G.D.C., and Nieuwstadt, F.T.M., *Drag Reduction by Polymer Additives in a Turbulent Pipe Flow: Numerical and Laboratory Experiments,* J. Fluid Mech., 337, pp.193-231, 1997.

Escudier, M.P., Presti, F., Smith, S., *Drag Reduction in the Turbulent Pipe Flow of Polymers*, J. Non-Newtonian Fluid Mech., 81, pp. 197-213, 1999.

Gasljevic, K., Aguilar, G., Matthys, E.F., *An Improved Diameter Scaling Correlation for Turbulent Flow of Drag-Reducing Polymer Solutions*, J. Non-Newtonian Fluid Mech., 84, pp. 131-148, 1999.

Gyr, A., Tsinober, A., *On the Rheological Nature of Drag Reduction Phenomena*, J. Non-Newtonian Fluid Mech., 73, pp. 153-162, 1997.

Hinch, E.J., *Mechanical Models of Dilute Polymer Solutions in Strong Flows*, The Physics of Fluids, 20 (10), pp. S22-S30, 1977.

Hinze, J.O., *Turbulence; An Introduction to the Its Mechanism and Theory*, McGraw-Hill, New York, 1959.

Landahl, M.T., *Dynamics of Boundary Layer Turbulence and the Mechanism of Drag Reduction*, The Physics of Fluids, 20 (10), pp. S55-S63, 1977.

Liberatore, M.W., Baik, S., McHugh, A.J., Hanratty, T.J., *Turbulent Drag Reduction of Polyacrylamide Solutions: Effect of Degradation on Molecular Weight Distribution*, J. Non-Newtonian Fluid Mech., 123, pp. 175-183, 2004.

Lumley, J.L., *Drag Reduction by Additives*, Ann. Rev. Fluid Mech., 1, pp. 367-383, 1969.

Lumley, J.L., *Drag Reduction in Turbulent Flow by Polymer Additives*, J. Polymer Sci.: Macromol. Rev., 7, pp. 263-290, 1973.

Min, T., Choi, H., and Yoo, J.Y., *Maximum Drag Reduction in a Turbulent channel flow by Polymer Additives*, J. Fluid Mech., 492, pp. 91-100, 2003.

Myska, J., and Zakin, J.L., *Difference in the Flow Behaviors of Polymeric and Cationic Surfactant Drag-Reducing Additives*, Ind. Eng. Chem. Res., 36, pp. 5483-5487, 1997.

Myska, J., Lin, Z., Stepanek, P., Zakin, J.L., *Influence of Salts on Dynamic Properties of Drag Reducing Surfactants*, J. Non-Newtonian Fluid Mech., 97, pp. 251-266, 2001.

Pinho, F.T., and Whitelaw, J.H., *Flow of Non-Newtonian Fluids in a Pipe*, J. Non-Newtonian Fluid Mech., 34, pp. 129-144, 1990.

Ptasinski, P.K., Nieuwstadt, F.T.M., Van Den Brule, B.H.A.A., and Hulsen, M.A., *Experiments in Turbulent Pipe Flow with Polymer Additives at Maximum Drag Reduction, Flow*, Turbulence and Combustion, 66, pp. 159-182, 2001.

Ryskin, G., *Turbulent Drag Reduction by Polymers: A Quantitative Theory*, Physical Review Letters, 59(18), pp. 2059-2062, 1987.

Sá Pereira, A., Pinho, F.T., *Turbulent Pipe Flow Characteristics of Low Molecular Weight Polymer Solutions*, J. Non-Newtonian Fluid Mech., 55, pp. 321-344, 1994.

Signal-Processing, http://www.signal-processing.com, last accessed able, August 2005.

Toms, B.A., *Some Observation on the Flow of Linear Polymer Solutions through Straight Tubes at Large Reynolds Number*, in: Proceedings of the First International Congress of Rheology, North Holland, Amsterdam, 2, pp. 135-141, 1949.

Usui, H., Maeguchi, K., and Sano, Y., *Drag Reduction Caused by the Injection of Polymer Thread into a Turbulent Pipe Flow*, Phys. Fluids, 31, pp. 2518-2523, 1988.

Van Dam, P.H.J., Wegdam, G.H., Van Der Elsken, J., *The Structure of Turbulence in a Dilute Polymer Solutions*, J. Non-Newtonian Fluid Mech., 53, pp. 215-225, 1994.

Virk, P.S., Merrill, E.W., Mickley, H.S., Smith, K.A., *The Toms Phenomenon: turbulent pipe flow of dilute polymer solutions*, J. Fluid Mech. 30, pp. 305-328, 1967.

Virk, P.S., *Drag Reduction Fundamentals*, AIChE Journal, 21, pp. 625-656, 1975.

Warholic, M.D., Massah, H., Hanratty, T.J., *Influence of Drag-Reducing on Turbulence: Effects of Reynolds Number, Concentration and Mixing*, Experiments in Fluids, 27, pp. 461-472, 1999.

Warholic, M.D., Heist, D.K., Katcher, M., Hanratty, T.J., *A Study with Particle-Image Velocimetry of the influence of Drag-Reducing Polymers on the Structure of Turbulence*, Experiments in Fluids, 31, pp. 474-483, 2001.

Wei, T., and Willmarth W.W., *Modifying Turbulent Structure with Drag-Reducing Polymer Additives in Turbulent Pipe Flow*, J. Fluid Mech., 245, pp. 619-641, 1992.

Wilcox, D.C., *Turbulence Modeling for CFD*, 2nd Ed., La Canada, Calif., DCW Industries, 1998.

Willemetz, J.C., *Signal Processing – DOP2000 User's Manuel*, Signal Processing S.A., Switzerland.

Wójs, K., *Laminar and Turbulent Flow of Dilute Polymer Solutions in Smooth and Rough Pipes*, J. Non-Newtonian Fluid Mech., 48, pp. 337-355, 1993.

Yu, B., Li, F., Kawaguchi, Y., *Numerical and Experimental Investigation of Turbulent Characteristics in a Drag-Reducing Flow with Surfactant Additives*, International Journal of Heat and Fluid Flow, 25, pp. 961-974, 2004.

Zakin, J.L., and Hunston, D.L., *Effect of Polymer Molecular Variables on Drag Reduction*, J. Macromol. Sci. Phys., B18(4), pp. 795-814, 1980.

APPENDIX A

FLOW PROPERTIES

A.1 Flow Properties of Solutions

Table A.1.1 Flow properties of water.

Q, l/s	<V>, m/s	Re	ΔP, Pa	τ_w, kg/m^2	f
0.909	0.547	24585	302.8347	0.87065	0.005938
0.833	0.501	22518	266.783	0.767001	0.006236
0.714	0.43	19326	199.4864	0.573523	0.00633
0.667	0.401	18023	180.2588	0.518244	0.006577
0.625	0.376	16899	161.0312	0.462965	0.006683
0.588	0.354	15911	146.6105	0.421505	0.006864
0.556	0.335	15057	129.7863	0.373136	0.006785
0.5	0.301	13529	112.9622	0.324766	0.007315
0.455	0.274	12315	93.73455	0.269487	0.007326
0.417	0.251	11281	79.31385	0.228027	0.007387
0.385	0.232	10427	69.70005	0.200388	0.007598
0.333	0.2	8989	52.8759	0.152018	0.007756
0.313	0.188	8450	48.069	0.138198	0.00798
0.278	0.167	7506	38.4552	0.110559	0.00809
0.244	0.147	6607	31.24485	0.089829	0.008484

Table A.1.2 Flow properties of 200 wppm CMC.

Q, l/s	<V>, m/s	Re	ΔP, Pa	τ_w, kg/m^2	f
0.909	0.547	20612	298.5919	0.858452	0.005837
0.833	0.501	18879	260.3721	0.74857	0.006068
0.714	0.43	16203	200.6537	0.57688	0.006348
0.667	0.401	15110	181.5439	0.521939	0.006604
0.625	0.376	14168	164.8227	0.473865	0.00682
0.588	0.354	13339	150.4903	0.43266	0.007025
0.556	0.335	12623	136.1579	0.391454	0.007097
0.5	0.301	11342	112.2705	0.322778	0.007248
0.455	0.274	10325	96.98264	0.278825	0.007556
0.417	0.251	9458	82.65023	0.237619	0.007674
0.385	0.232	8742	71.66205	0.206028	0.007788
0.333	0.2	7536	54.94091	0.157955	0.008034
0.294	0.177	6670	45.38597	0.130485	0.008474
0.263	0.158	5954	37.26427	0.107135	0.008732

Table A.1.3 Flow properties of 300 wppm CMC.

Q. l/s	<V>, m/s	Re	ΔP, Pa	τ_w, kg/m^2	f
0.909	0.547	18322	293.8144	0.844716	0.005744
0.833	0.501	16781	255.5946	0.734835	0.005956
0.714	0.43	14403	205.4312	0.590615	0.006499
0.667	0.401	13431	183.9326	0.528806	0.006691
0.625	0.376	12594	167.2115	0.480733	0.006918
0.588	0.354	11857	150.4903	0.43266	0.007025
0.556	0.335	11221	138.5466	0.398322	0.007221
0.5	0.301	10082	114.6593	0.329645	0.007403

Table A.1.3 (continued)

0.455	0.274	9178	97.93814	0.281572	0.007631
0.417	0.251	8407	85.03897	0.244487	0.007896
0.385	0.232	7771	73.57304	0.211522	0.007996
0.333	0.2	6699	57.32964	0.164823	0.008384
0.294	0.177	5929	47.7747	0.137352	0.00892
0.278	0.167	5594	42.99723	0.123617	0.009018

Table A.1.4 Flow properties of 400 wppm CMC.

Q, l/s	<V>, m/s	Re	ΔP, Pa	τ_w, kg/m^2	f
0.909	0.547	15021	294.9867	0.848087	0.005755
0.833	0.501	13758	271.1975	0.779693	0.006307
0.714	0.43	11808	209.3454	0.601868	0.006609
0.667	0.401	11012	190.314	0.547153	0.006909
0.625	0.376	10325	173.6615	0.499277	0.007171
0.588	0.354	9721	157.0091	0.451401	0.007314
0.556	0.335	9199	145.1144	0.417204	0.007548
0.5	0.301	8266	121.3252	0.34881	0.007817
0.455	0.274	7524	102.2938	0.294095	0.007954
0.417	0.251	6893	88.02023	0.253058	0.008156
0.385	0.232	6371	77.55296	0.222965	0.008411
0.333	0.2	5492	64.23098	0.184664	0.009374

Table A.1.5 Flow properties of 500 wppm CMC .

Q, l/s	<V>, m/s	Re	ΔP, Pa	τ_w, kg/m^2	f
0.909	0.547	13769	290.2289	0.834408	0.005662
0.833	0.501	12611	256.9239	0.738656	0.005975
0.714	0.43	10824	202.2086	0.58135	0.006384
0.667	0.401	10094	187.9351	0.540313	0.006823
0.625	0.376	9465	171.2826	0.492437	0.007072
0.588	0.354	8911	161.7669	0.46508	0.007536
0.556	0.335	8433	147.4934	0.424043	0.007672
0.5	0.301	7577	121.3252	0.34881	0.007817
0.455	0.274	6897	104.6727	0.300934	0.008139
0.417	0.251	6318	89.44758	0.257162	0.008288
0.385	0.232	5840	79.4561	0.228436	0.008618
0.333	0.2	5034	61.85205	0.177825	0.009027

APPENDIX B

ULTRASOUND DOPPLER PARAMETERS

B.1 UDV Parameters Used in the Experiments

Table B.1.1 UDV Parameters.

	Water	200 wppm CMC	300 wppm CMC	400 wppm CMC	500 wppm CMC
PRF, Hz	7246	7812	7246	7246	7246
Emitting Power	Low	Low	Low	Low	Low
Burst Length, cycles	8	8	8	8	8
Emitting Frequency, MHz	4.000	4.000	4.000	4.000	4.000
Resolution, mm	0.37	0.37	0.37	0.37	0.37
Sensitivity	Very High	Very High	Very High	Very High	Very High
Number of Gates	192	192	192	192	192
TGC Mode	Uniform	Uniform	Uniform	Uniform	Uniform
TGC, dB	55	41	51	50	50

Table B.1.1 (continued)

Profiles to Record	128	128	128	128	128
Acquisition Time, s	0.04	0.03	0.04	0.04	0.04
Sound speed, m/s	1490	1490	1490	1490	1490
Applied Filter	None	None	None	None	None

APPENDIX C

VELOCITY PROFILE DATA

C.1 Velocity Profile Data for <V>=0.547 m/s

Table C.1.1 Velocity profile data for water at <V>=0.547 m/s.

r/R	$\bar{U}/\bar{U}_o$	u^+	y^+
0.8696	0.772397	16.08353	88.3176
0.8543	0.797899	16.61456	98.62132
0.8391	0.822483	17.12647	108.925
0.8239	0.835967	17.40725	119.2288
0.8087	0.846761	17.632	129.5325
0.7935	0.866883	18.05099	139.8362
0.7783	0.875824	18.23717	150.1399
0.763	0.881833	18.36229	160.4436
0.7478	0.887294	18.47601	170.7474
0.7326	0.895897	18.65515	181.0511
0.7174	0.902792	18.79873	191.3548
0.7022	0.909961	18.948	201.6585
0.687	0.912667	19.00436	211.9622
0.6717	0.914133	19.03489	222.266
0.6565	0.918096	19.11741	232.5697
0.6413	0.917565	19.10634	242.8734
0.6261	0.920577	19.16907	253.1771

Table C.1.1 (continued)

0.6109	0.92504	19.26199	263.4808
0.5957	0.932241	19.41194	273.7846
0.5804	0.935173	19.473	284.0883
0.5652	0.942181	19.61892	294.392
0.55	0.94616	19.70178	304.6957
0.5348	0.947191	19.72325	314.9994
0.5196	0.951267	19.80812	325.3032
0.5043	0.960128	19.99262	335.6069
0.4891	0.960369	19.99765	345.9106
0.4739	0.963817	20.06944	356.2143
0.4587	0.964107	20.07548	366.518
0.4435	0.967232	20.14056	376.8218
0.4283	0.975126	20.30493	387.1255
0.413	0.97801	20.36498	397.4292
0.3978	0.97656	20.33479	407.7329
0.3826	0.981635	20.44046	418.0366
0.3674	0.983906	20.48776	428.3404
0.3522	0.98679	20.5478	438.6441
0.337	0.99122	20.64005	448.9478
0.3217	0.991736	20.65079	459.2515
0.3065	0.992154	20.65951	469.5552
0.2913	0.99507	20.72023	479.859
0.2761	0.997422	20.7692	490.1627
0.2609	0.999984	20.82254	500.4664
0.2457	1	20.82288	510.7701
0.2304	1	20.82288	521.0738
0.2152	1	20.82288	531.3776
0.2	1	20.82288	541.6813
0.1848	1	20.82288	551.985
0.1696	1	20.82288	562.2887

Table C.1.1 (continued)

0.1543	1	20.82288	572.5924
0.1391	1	20.82288	582.8962
0.1239	1	20.82288	593.1999
0.1087	1	20.82288	603.5036
0.0935	1	20.82288	613.8073
0.0783	1	20.82288	624.111
0.063	1	20.82288	634.4148
0.0478	1	20.82288	644.7185
0.0326	1	20.82288	655.0222
0.0174	1	20.82288	665.3259
0	1	20.82288	677.1016

Table C.1.2 Velocity profile data for 200 wppm CMC at <V>=0.547 m/s.

r/R	$\bar{U}/\bar{U}_o$	u^+	y^+
0.8713	0.750943	16.16142	71.65087
0.8565	0.767863	16.52555	79.88104
0.8413	0.782974	16.85076	88.35327
0.8261	0.807425	17.37699	96.8255
0.8109	0.82024	17.65279	105.2977
0.7961	0.836232	17.99695	113.5279
0.7809	0.848512	18.26125	122.0001
0.7657	0.853403	18.3665	130.4724
0.7504	0.860557	18.52047	138.9446
0.7352	0.868011	18.68088	147.4168
0.7204	0.877964	18.89509	155.647
0.7052	0.885905	19.06599	164.1192
0.69	0.892808	19.21455	172.5915

Table C.1.2 (continued)

0.6748	0.894852	19.25854	181.0637
0.66	0.89828	19.33232	189.2939
0.6448	0.907777	19.53672	197.7661
0.6296	0.91284	19.64569	206.2383
0.6143	0.919806	19.7956	214.7105
0.5991	0.924225	19.89069	223.1828
0.5843	0.927039	19.95127	231.4129
0.5691	0.932669	20.07242	239.8852
0.5539	0.937087	20.16751	248.3574
0.5387	0.939493	20.21929	256.8296
0.5239	0.944037	20.31709	265.0598
0.5087	0.948833	20.4203	273.532
0.4935	0.949792	20.44095	282.0043
0.4783	0.95462	20.54484	290.4765
0.463	0.956648	20.58849	298.9487
0.4483	0.958661	20.63181	307.1789
0.433	0.961193	20.68629	315.6511
0.4178	0.969794	20.8714	324.1234
0.4026	0.97275	20.93503	332.5956
0.3878	0.97363	20.95398	340.8258
0.3726	0.979008	21.06971	349.298
0.3574	0.980455	21.10085	357.7702
0.3422	0.986791	21.2372	366.2425
0.3274	0.989323	21.29171	374.4726
0.3122	0.990952	21.32676	382.9449
0.297	0.99169	21.34265	391.4171
0.2817	0.992706	21.36452	399.8893
0.2665	0.994349	21.39987	408.3615
0.2517	0.998245	21.48373	416.5917
0.2365	0.99851	21.48943	425.0639

Table C.1.2 (continued)

0.2213	0.99897	21.49932	433.5362
0.2061	0.998747	21.49453	442.0084
0.1913	1	21.52149	450.2386
0.1761	1	21.52149	458.7108
0.1609	1	21.52149	467.183
0.1457	1	21.52149	475.6553
0.1304	1	21.52149	484.1275
0.1157	1	21.52149	492.3577
0.1004	1	21.52149	500.8299
0.0852	1	21.52149	509.3021
0.07	1	21.52149	517.7744
0.0552	1	21.52149	526.0045
0.04	1	21.52149	534.4768
0.0248	1	21.52149	542.949
0.0096	1	21.52149	551.4212
0	1	21.52149	556.7466

Table C.1.3 Velocity profile data for 300 wppm CMC at <V>=0.547 m/s.

r/R	$\bar{U}/\bar{U}_o$	u^+	y^+
0.8696	0.729064	15.83419	64.55033
0.8543	0.746642	16.21597	72.08121
0.8391	0.76499	16.61447	79.61208
0.8239	0.778469	16.9072	87.14295
0.8087	0.801797	17.41385	94.67382
0.7935	0.812998	17.65711	102.2047
0.7783	0.829759	18.02115	109.7356
0.763	0.834834	18.13135	117.2664

Table C.1.3 (continued)

0.7478	0.84495	18.35107	124.7973
0.7326	0.849946	18.45957	132.3282
0.7174	0.860063	18.67929	139.8591
0.7022	0.868373	18.85977	147.3899
0.687	0.873918	18.98021	154.9208
0.6717	0.878128	19.07165	162.4517
0.6565	0.885998	19.24258	169.9825
0.6413	0.894528	19.42784	177.5134
0.6261	0.898817	19.52098	185.0443
0.6109	0.903734	19.62777	192.5752
0.5957	0.914825	19.86865	200.106
0.5804	0.92447	20.07813	207.6369
0.5652	0.930471	20.20846	215.1678
0.55	0.932906	20.26134	222.6987
0.5348	0.936943	20.34903	230.2295
0.5196	0.941578	20.44968	237.7604
0.5043	0.946746	20.56192	245.2913
0.4891	0.947594	20.58035	252.8221
0.4739	0.949008	20.61105	260.353
0.4587	0.953359	20.70556	267.8839
0.4435	0.953359	20.70556	275.4148
0.4283	0.957994	20.80622	282.9456
0.413	0.965089	20.96031	290.4765
0.3978	0.969344	21.05273	298.0074
0.3826	0.975588	21.18834	305.5382
0.3674	0.976723	21.21299	313.0691
0.3522	0.978142	21.24381	320.6
0.337	0.978804	21.25817	328.1309
0.3217	0.983533	21.36089	335.6617
0.3065	0.983534	21.3609	343.1926

Table C.1.3 (continued)

0.2913	0.987884	21.45538	350.7235
0.2761	0.987978	21.45742	358.2544
0.2609	0.993654	21.5807	365.7852
0.2457	0.998857	21.6937	373.3161
0.2304	1	21.71853	380.847
0.2152	1	21.71853	388.3778
0.2	1	21.71853	395.9087
0.1848	1	21.71853	403.4396
0.1696	1	21.71853	410.9705
0.1543	1	21.71853	418.5013
0.1391	1	21.71853	426.0322
0.1239	1	21.71853	433.5631
0.1087	1	21.71853	441.0939
0.0935	1	21.71853	448.6248
0.0783	1	21.71853	456.1557
0.063	1	21.71853	463.6866
0.0478	1	21.71853	471.2174
0.0326	1	21.71853	478.7483
0.0174	1	21.71853	486.2792
0	1	21.71853	494.8859

Table C.1.4 Velocity profile data for 400 wppm CMC at <V>=0.547 m/s.

r/R	$\bar{U}/\bar{U}_o$	u^+	y^+
0.8713	0.696872	15.13974	51.84467
0.8565	0.711995	15.4683	57.7998
0.8413	0.730068	15.86094	63.93008
0.8261	0.747231	16.23381	70.06036

Table C.1.4 (continued)

0.8109	0.767124	16.66599	76.19065
0.7961	0.788993	17.1411	82.14578
0.7809	0.798955	17.35753	88.27606
0.7657	0.81127	17.62509	94.40634
0.7504	0.818362	17.77914	100.5366
0.7352	0.826017	17.94547	106.6669
0.7204	0.837297	18.19052	112.622
0.7052	0.843855	18.33299	118.7523
0.69	0.851683	18.50307	124.8826
0.6748	0.859229	18.66701	131.0129
0.66	0.865175	18.79618	136.968
0.6448	0.871811	18.94035	143.0983
0.6296	0.878134	19.07771	149.2286
0.6143	0.885633	19.24063	155.3589
0.5991	0.892881	19.39809	161.4891
0.5843	0.898983	19.53067	167.4443
0.5691	0.905635	19.67519	173.5746
0.5539	0.914546	19.86878	179.7048
0.5387	0.921418	20.01806	185.8351
0.5239	0.929654	20.197	191.7902
0.5087	0.934721	20.30709	197.9205
0.4935	0.943789	20.50409	204.0508
0.4783	0.947288	20.5801	210.1811
0.463	0.948637	20.60941	216.3114
0.4483	0.949468	20.62747	222.2665
0.433	0.953282	20.71034	228.3968
0.4178	0.956348	20.77694	234.5271
0.4026	0.959413	20.84352	240.6573
0.3878	0.962659	20.91404	246.6125
0.3726	0.964461	20.9532	252.7428

Table C.1.4 (continued)

0.3574	0.965796	20.98221	258.873
0.3422	0.966968	21.00766	265.0033
0.3274	0.969041	21.05269	270.9585
0.3122	0.972467	21.12714	277.0887
0.297	0.973062	21.14006	283.219
0.2817	0.975082	21.18394	289.3493
0.2665	0.9773	21.23212	295.4796
0.2517	0.979156	21.27245	301.4347
0.2365	0.985107	21.40173	307.565
0.2213	0.991868	21.54863	313.6953
0.2061	1	21.72529	319.8256
0.1913	1	21.72529	325.7807
0.1761	1	21.72529	331.911
0.1609	1	21.72529	338.0413
0.1457	1	21.72529	344.1715
0.1304	1	21.72529	350.3018
0.1157	1	21.72529	356.2569
0.1004	1	21.72529	362.3872
0.0852	1	21.72529	368.5175
0.07	1	21.72529	374.6478
0.0552	1	21.72529	380.6029
0.04	1	21.72529	386.7332
0.0248	1	21.72529	392.8635
0.0096	1	21.72529	398.9938
0	1	21.72529	402.8471

Table C.1.5 Velocity profile data for 500 wppm CMC at <V>=0.547 m/s.

r/R	$\bar{U}/\bar{U}_o$	u^+	y^+
0.8696	0.673876	14.75953	48.1665
0.8543	0.690125	15.11542	53.78593
0.8391	0.700916	15.35177	59.40535
0.8239	0.714828	15.65648	65.02478
0.8087	0.732818	16.0505	70.6442
0.7935	0.750384	16.43525	76.26363
0.7783	0.767998	16.82102	81.88305
0.763	0.780906	17.10374	87.50248
0.7478	0.794049	17.39162	93.1219
0.7326	0.802064	17.56716	98.74133
0.7174	0.813733	17.82274	104.3608
0.7022	0.824038	18.04844	109.9802
0.687	0.832319	18.22982	115.5996
0.6717	0.840444	18.40776	121.219
0.6565	0.847	18.55136	126.8385
0.6413	0.854654	18.719	132.4579
0.6261	0.864472	18.93404	138.0773
0.6109	0.874259	19.1484	143.6967
0.5957	0.881756	19.31261	149.3162
0.5804	0.890555	19.50532	154.9356
0.5652	0.89628	19.63071	160.555
0.55	0.903275	19.78392	166.1744
0.5348	0.908968	19.90862	171.7939
0.5196	0.917187	20.08863	177.4133
0.5043	0.925092	20.26177	183.0327
0.4891	0.93444	20.46651	188.6521
0.4739	0.944556	20.68808	194.2716
0.4587	0.947661	20.7561	199.891

Table C.1.5 (continued)

0.4435	0.949481	20.79595	205.5104
0.4283	0.951316	20.83614	211.1298
0.413	0.953355	20.8808	216.7493
0.3978	0.957213	20.9653	222.3687
0.3826	0.961401	21.05703	227.9881
0.3674	0.963252	21.09756	233.6075
0.3522	0.966734	21.17382	239.227
0.337	0.9678	21.19718	244.8464
0.3217	0.97216	21.29268	250.4658
0.3065	0.973039	21.31192	256.0852
0.2913	0.975862	21.37375	261.7047
0.2761	0.977117	21.40124	267.3241
0.2609	0.978842	21.43902	272.9435
0.2457	0.982418	21.51735	278.5629
0.2304	0.984378	21.56029	284.1824
0.2152	0.986292	21.6022	289.8018
0.2	0.988268	21.64548	295.4212
0.1848	0.98868	21.65451	301.0406
0.1696	0.993308	21.75587	306.6601
0.1543	1	21.90244	312.2795
0.1391	1	21.90244	317.8989
0.1239	1	21.90244	323.5183
0.1087	1	21.90244	329.1378
0.0935	1	21.90244	334.7572
0.0783	1	21.90244	340.3766
0.063	1	21.90244	345.996
0.0478	1	21.90244	351.6155
0.0326	1	21.90244	357.2349
0.0174	1	21.90244	362.8543
0	1	21.90244	369.2765

APPENDIX D

AXIAL TURBULENT INTENSITIES AND EDDY VISCOSITIES

D.1. Axial Turbulent Intensities and Eddy Viscosities for <V>=0.547 m/s

Table D.1.1 Axial turbulent intensities and Eddy viscosities for water.

r/R	u'_{rms}	ε	ε/μ
0.8696	91.5148	0.025168	25.09231
0.8543	90.28	0.026991	26.91051
0.8391	88.7718	0.028945	28.8584
0.8239	88.7514	0.031034	30.94159
0.8087	86.5103	0.033264	33.16472
0.7935	81.5736	0.035638	35.53112
0.7783	75.6132	0.038157	38.04237
0.763	67.051	0.04082	40.6978
0.7478	62.932	0.043624	43.49394
0.7326	62.3493	0.046563	46.424
0.7174	60.2794	0.049626	49.47727
0.7022	56.0132	0.052797	52.63861
0.687	51.0632	0.056056	55.88808
0.6717	49.7292	0.059378	59.20066
0.6565	49.0239	0.062734	62.54628
0.6413	46.7503	0.066088	65.8901
0.6261	43.7705	0.069401	69.19321

Table D.1.1 (continued)

0.6109	41.3969	0.072631	72.41364
0.5957	41.4897	0.075734	75.50779
0.5804	42.8685	0.078667	78.43218
0.5652	43.4058	0.081389	81.1453
0.55	45.2791	0.08386	83.60967
0.5348	43.3195	0.086051	85.79355
0.5196	41.6911	0.087936	87.67256
0.5043	42.6838	0.089498	89.23068
0.4891	42.627	0.090732	90.46078
0.4739	42.0128	0.091639	91.36454
0.4587	41.3728	0.092228	91.95186
0.4435	40.5288	0.092517	92.23983
0.4283	40.7854	0.092528	92.25134
0.413	40.4298	0.09229	92.01359
0.3978	39.2588	0.091831	91.55655
0.3826	38.8206	0.091184	90.91158
0.3674	38.9567	0.09038	90.11011
0.3522	39.251	0.08945	89.18267
0.337	37.8423	0.088423	88.15811
0.3217	35.4718	0.087324	87.06306
0.3065	35.3316	0.086179	85.9216
0.2913	36.4631	0.085009	84.75515
0.2761	38.0801	0.083833	83.58241
0.2609	38.9893	0.082667	82.41952
0.2457	39.7834	0.081524	81.28018
0.2304	42.0896	0.080416	80.17591
0.2152	44.3702	0.079354	79.11623
0.2	44.4418	0.078343	78.10897
0.1848	43.731	0.077392	77.16044
0.1696	42.7926	0.076505	76.27568

Table D.1.1 (continued)

0.1543	41.4174	0.075685	75.45869
0.1391	39.2276	0.074937	74.71255
0.1239	37.4701	0.074262	74.03965
0.1087	38.2966	0.073662	73.44177
0.0935	41.3403	0.073139	72.92024
0.0783	43.5451	0.072693	72.47603
0.063	44.927	0.072326	72.10981
0.0478	42.4312	0.072038	71.82207
0.0326	39.1857	0.071828	71.61311
0.0174	37.1101	0.071698	71.48314
0	37.1557	#SAYI/0!	#SAYI/0!

Table D.1.2 Axial turbulent intensities and Eddy viscosities for 200 wppm CMC.

r/R	u'_{rms}	ε	ε/μ
0.8713	77.2353	0.023181	19.31717
0.8565	77.1109	0.024565	20.47061
0.8413	75.5214	0.026065	21.72123
0.8261	72.9438	0.027644	23.03684
0.8109	69.9226	0.029301	24.41768
0.7961	61.4422	0.030985	25.82106
0.7809	54.6739	0.032794	27.32822
0.7657	50.5135	0.034676	28.8965
0.7504	48.0781	0.036627	30.52248
0.7352	45.4009	0.038642	32.20152
0.7204	43.1159	0.040653	33.87775
0.7052	45.4786	0.042771	35.6426
0.69	47.5901	0.044926	37.43869

Table D.1.2 (continued)

0.6748	48.1276	0.047107	39.2559
0.66	47.9473	0.049237	41.03057
0.6448	45.6772	0.051426	42.85479
0.6296	42.6254	0.053595	44.66289
0.6143	41.616	0.055729	46.44062
0.5991	41.6151	0.057808	48.17337
0.5843	39.8559	0.05976	49.79973
0.5691	38.7777	0.061682	51.40157
0.5539	38.417	0.0635	52.91686
0.5387	37.9386	0.0652	54.33362
0.5239	37.3793	0.066727	55.60574
0.5087	37.2536	0.06816	56.79983
0.4935	37.2129	0.069445	57.87063
0.4783	38.5283	0.070577	58.81421
0.463	38.3459	0.071555	59.629
0.4483	37.6878	0.072357	60.29783
0.433	36.3622	0.073035	60.86281
0.4178	36.3558	0.073569	61.30718
0.4026	39.256	0.073965	61.63731
0.3878	40.4079	0.074227	61.85596
0.3726	39.4286	0.074381	61.98454
0.3574	39.3589	0.07443	62.02461
0.3422	38.0131	0.074383	61.98609
0.3274	38.696	0.07426	61.88295
0.3122	39.6916	0.074063	61.71891
0.297	41.3214	0.073807	61.50583
0.2817	40.1758	0.073504	61.25307
0.2665	38.3011	0.073163	60.96946
0.2517	36.6945	0.072807	60.67225
0.2365	36.1458	0.072422	60.35139

Table D.1.2 (continued)

0.2213	36.1872	0.072027	60.02226
0.2061	36.4402	0.071629	59.69118
0.1913	35.5876	0.071248	59.37301
0.1761	35.4777	0.070865	59.05394
0.1609	35.7501	0.070497	58.74784
0.1457	35.3026	0.07015	58.45856
0.1304	35.2551	0.069827	58.18947
0.1157	35.9281	0.06954	57.95014
0.1004	34.819	0.069275	57.72889
0.0852	34.5803	0.069042	57.53517
0.07	35.1317	0.068845	57.37069
0.0552	35.4601	0.068688	57.24023
0.04	36.5638	0.068565	57.13716
0.0248	35.9772	0.06848	57.06656
0.0096	33.8833	0.068435	57.02898
0	32.0196	#SAYI/0!	#SAYI/0!

Table D.1.3 Axial turbulent intensities and Eddy viscosities for 300 wppm CMC.

r/R	u'_{rms}	ε	ε/μ
0.8696	103.9798	0.022403	16.59476
0.8543	103.4968	0.023563	17.45399
0.8391	102.7827	0.02477	18.34801
0.8239	99.3073	0.026023	19.27647
0.8087	98.057	0.027322	20.23871
0.7935	98.1428	0.028666	21.23373
0.7783	95.2982	0.030051	22.2601
0.763	88.6611	0.031477	23.31601

Table D.1.3 (continued)

0.7478	83.8522	0.032939	24.39919
0.7326	79.2292	0.034434	25.5069
0.7174	72.1502	0.035959	26.63594
0.7022	65.0168	0.037507	27.78263
0.687	61.2861	0.039073	28.94282
0.6717	62.1622	0.040651	30.11195
0.6565	67.2818	0.042235	31.28505
0.6413	70.7918	0.043817	32.45681
0.6261	71.6169	0.045389	33.62168
0.6109	68.175	0.046945	34.77389
0.5957	63.3778	0.048475	35.90763
0.5804	56.8914	0.049973	37.01709
0.5652	51.6367	0.05143	38.09659
0.55	46.4458	0.05284	39.14072
0.5348	42.7461	0.054195	40.1444
0.5196	40.1012	0.055489	41.10305
0.5043	38.2217	0.056717	42.0126
0.4891	37.8928	0.057874	42.86964
0.4739	36.7541	0.058956	43.67145
0.4587	37.0655	0.059962	44.416
0.4435	37.2002	0.060888	45.10204
0.4283	38.4896	0.061734	45.72904
0.413	39.8123	0.062501	46.2972
0.3978	40.6412	0.06319	46.80738
0.3826	40.3028	0.063802	47.26105
0.3674	40.5502	0.064341	47.66026
0.3522	38.6608	0.06481	48.00752
0.337	37.9343	0.065213	48.30574
0.3217	39.4579	0.065553	48.55813
0.3065	38.9242	0.065837	48.76816

Table D.1.3 (continued)

0.2913	38.0189	0.066068	48.93944
0.2761	39.419	0.066252	49.07568
0.2609	41.0323	0.066394	49.18062
0.2457	40.6086	0.066498	49.25793
0.2304	38.7401	0.06657	49.31124
0.2152	36.9098	0.066614	49.34403
0.2	37.3044	0.066635	49.35963
0.1848	36.7038	0.066638	49.36119
0.1696	35.8585	0.066625	49.35165
0.1543	33.6362	0.066601	49.33373
0.1391	32.2744	0.066568	49.30993
0.1239	33.1615	0.066531	49.28249
0.1087	33.9427	0.066492	49.25345
0.0935	34.2392	0.066453	49.22456
0.0783	35.6187	0.066416	49.19738
0.063	36.127	0.066384	49.17319
0.0478	34.9143	0.066357	49.15307
0.0326	34.7307	0.066336	49.13784
0.0174	33.2956	0.066323	49.12811
0	31.5834	#SAYI/0!	#SAYI/0!

Table D.1.4 Axial turbulent intensities and Eddy viscosities for 400 wppm CMC.

r/R	u'_{rms}	ε	ε/μ
0.8713	83.5484	0.019937	12.08329
0.8565	89.6475	0.020999	12.72684
0.8413	91.5718	0.022135	13.41532
0.8261	91.7356	0.023314	14.1295

Table D.1.4 (continued)

0.8109	91.7066	0.024533	14.86837
0.7961	90.179	0.025754	15.60848
0.7809	84.0227	0.027046	16.39164
0.7657	78.9434	0.02837	17.19424
0.7504	75.1889	0.029723	18.01368
0.7352	72.5472	0.031097	18.84691
0.7204	70.0991	0.032449	19.66626
0.7052	65.5056	0.033852	20.51613
0.69	60.0345	0.035258	21.3683
0.6748	54.788	0.03666	22.21819
0.66	51.6941	0.038011	23.03703
0.6448	49.4047	0.039382	23.86809
0.6296	46.8455	0.040725	24.68206
0.6143	44.6726	0.042032	25.47386
0.5991	45.6537	0.043294	26.23855
0.5843	45.6135	0.044469	26.95097
0.5691	44.8071	0.045621	27.64879
0.5539	43.3794	0.046706	28.3067
0.5387	45.6184	0.04772	28.92136
0.5239	46.7865	0.048633	29.47446
0.5087	45.582	0.049494	29.99654
0.4935	45.0477	0.050274	30.46931
0.4783	44.4464	0.050972	30.89212
0.463	44.0751	0.051587	31.26505
0.4483	45.5862	0.052107	31.58021
0.433	47.6012	0.052565	31.85745
0.4178	48.9901	0.052946	32.08863
0.4026	47.311	0.053256	32.27609
0.3878	46.6265	0.053491	32.41887
0.3726	45.5532	0.053672	32.52832

Table D.1.4 (continued)

0.3574	46.8072	0.053795	32.60286
0.3422	47.34	0.053866	32.64586
0.3274	46.859	0.05389	32.66068
0.3122	45.9265	0.053875	32.65154
0.297	46.5277	0.053825	32.62102
0.2817	46.0483	0.053744	32.57241
0.2665	45.9157	0.05364	32.50887
0.2517	48.879	0.053519	32.43572
0.2365	49.4873	0.05338	32.3514
0.2213	46.1092	0.05323	32.26057
0.2061	47.6878	0.053073	32.16566
0.1913	48.9517	0.052918	32.07168
0.1761	45.6717	0.052759	31.9751
0.1609	42.5897	0.052603	31.8805
0.1457	42.1166	0.052453	31.78954
0.1304	42.5835	0.052311	31.70367
0.1157	43.2372	0.052183	31.62635
0.1004	42.8161	0.052064	31.55414
0.0852	42.9045	0.051959	31.49035
0.07	43.5972	0.051869	31.4358
0.0552	43.8369	0.051797	31.39228
0.04	42.3323	0.05174	31.35775
0.0248	41.1498	0.051701	31.33402
0.0096	42.1333	0.05168	31.32136
0	43.1421	#SAYI/0!	#SAYI/0!

Table D.1.5 Axial turbulent intensities and Eddy viscosities for 500 wppm CMC.

r/R	u'_{rms}	ε	ε/μ
0.8696	106.4542	0.023937	13.29813
0.8543	113.893	0.024481	13.60066
0.8391	119.7147	0.025038	13.91013
0.8239	125.53	0.025608	14.22662
0.8087	126.7735	0.02619	14.5502
0.7935	121.2915	0.026786	14.88093
0.7783	113.5792	0.027394	15.21889
0.763	103.1373	0.028015	15.56409
0.7478	95.6675	0.02865	15.91658
0.7326	85.2882	0.029297	16.27636
0.7174	74.7725	0.029958	16.64343
0.7022	71.0717	0.030632	17.01775
0.687	66.4322	0.031319	17.39928
0.6717	61.4382	0.032018	17.78794
0.6565	60.0969	0.032731	18.18364
0.6413	58.3237	0.033455	18.58625
0.6261	53.7532	0.034192	18.9956
0.6109	48.5625	0.034941	19.41151
0.5957	48.7851	0.035701	19.83375
0.5804	48.0813	0.036472	20.26204
0.5652	49.7108	0.037253	20.69608
0.55	50.4003	0.038044	21.13552
0.5348	50.6093	0.038844	21.57996
0.5196	47.0979	0.039652	22.02895
0.5043	49.2928	0.040468	22.48199
0.4891	49.038	0.041289	22.93852
0.4739	47.9545	0.042116	23.39794
0.4587	46.5608	0.042947	23.85958

Table D.1.5 (continued)

0.4435	46.6257	0.043781	24.32271
0.4283	44.3775	0.044616	24.78655
0.413	44.1686	0.04545	25.25024
0.3978	45.3319	0.046283	25.71288
0.3826	47.2201	0.047112	26.17349
0.3674	48.0111	0.047936	26.63105
0.3522	51.3315	0.048752	27.08447
0.337	53.2551	0.049559	27.5326
0.3217	54.2041	0.050354	27.97425
0.3065	52.2965	0.051135	28.40818
0.2913	53.6426	0.0519	28.8331
0.2761	51.5661	0.052646	29.24769
0.2609	47.5196	0.053371	29.65059
0.2457	43.8395	0.054073	30.04044
0.2304	44.7847	0.054749	30.41585
0.2152	42.6424	0.055396	30.77544
0.2	41.8482	0.056012	31.11783
0.1848	38.7234	0.056595	31.44166
0.1696	39.5594	0.057142	31.74561
0.1543	38.1971	0.057651	32.02839
0.1391	41.1533	0.05812	32.28878
0.1239	42.2107	0.058546	32.52563
0.1087	43.7093	0.058928	32.73784
0.0935	42.1666	0.059264	32.92445
0.0783	39.1704	0.059552	33.08458
0.063	39.2723	0.059791	33.21744
0.0478	39.3631	0.05998	33.3224
0.0326	39.4165	0.060118	33.39895
0.0174	40.3558	0.060204	33.44671
0	40.6424	#SAYI/0!	#SAYI/0!